DOI: 10.1002/ejic.200600638

An Experimental and Density Functional Theory Approach Towards the Establishment of Preferential Metal- or Ligand-Based Electron-Transfer Processes in Large Quinonoid-Bridged Diruthenium Complexes $[\{(aap)_2Ru\}_2(\mu\text{-}BL^{2-})]^{n+}$ (aap = 2-Arylazopyridine)

Sandeep Ghumaan,[a] Sriparna Mukherjee,[a] Sanjib Kar,[a] Dipankar Roy,[a] Shaikh M. Mobin,[a] Raghavan B. Sunoj,*[a] and Goutam Kumar Lahiri*[a]

Keywords: Ruthenium / Bridging ligands / Radical ions / Density functional calculations / EPR spectroscopy

A group of ten quinonoid-bridged diruthenium(II) complexes $[(aap)_2Ru^{II}(\mu\text{-}BL_1^{2-})Ru^{II}(aap)_2](ClO_4)_2$, [**1a**–**1c**]$(ClO_4)_2$ and $[(pap)_2Ru^{II}(\mu\text{-}BL_n^{2-})Ru^{II}(pap)_2](ClO_4)_2$ [**2**–**8**]$(ClO_4)_2$ [aap = 2-arylazopyridine, NC_5H_4–N=N–C_6H_4(R) {R = H (pap) [**1a**]$(ClO_4)_2$, *m*-Me [**1b**]$(ClO_4)_2$, *m*-Cl [**1c**]$(ClO_4)_2$}; BL^{2-} = 5,8-dioxido-1,4-napthoquinone (BL_1^{2-}), 2,3-dichloro-5,8-dioxido-1,4-napthoquinone (BL_2^{2-}), 6,11-dioxido-5,12-naphthacenedione (BL_3^{2-}), 1,4-dioxido-9,10-anthraquinone (BL_4^{2-}), 2,3-dimethyl-1,4-dioxido-9,10-anthraquinone (BL_5^{2-}), 6,7-dichloro-1,4-dioxido-9,10-anthraquinone (BL_6^{2-}), 1,4-diimino-9,10-anthraquinone (BL_7^{2-}), 1,5-dioxido-9,10-anthraquinone (BL_8^{2-})] have been synthesized. The crystal structures of [**1a**]$(ClO_4)_2{\cdot}H_2O$ and [**3**]$(ClO_4)_2$ suggest the preferential crystallization of the *meso* isomer in both cases. The two similar C–O distances in coordinated BL_1^{2-} [C2–O1/C4–O2 1.278(5)/1.291(4) Å] and BL_3^{2-} [C2–O1/C4–O2 1.282(7)/1.280(7) Å] in [**1a**]$(ClO_4)_2$ and [**3**]$(ClO_4)_2$, respectively, and the corresponding intraring distances suggest a delocalized keto-enol state of the coordinated BL^{2-}. $[\mathbf{1}\text{–}\mathbf{8}]^{2+}$ exhibit two successive one-electron oxidation processes and multiple reductions in both CH_3CN and CH_2Cl_2. The first oxidation potential varies substantially depending on a variety of factors associated with BL^{2-} and follows the order: $[\mathbf{8}]^{2+} >> [\mathbf{2}]^{2+} > [\mathbf{6}]^{2+} > [\mathbf{1a}]^{2+} \geq [\mathbf{4}]^{2+} > [\mathbf{3}]^{2+} > [\mathbf{5}]^{2+} >> [\mathbf{7}]^{2+}$. The separation in potentials between the successive oxidation processes translates to comproportionation constant (K_c) values in the ranges 2.5×10^4–2.6×10^5 and 1.7×10^3–1.3×10^6 in CH_3CN and CH_2Cl_2, respectively. The intermediate paramagnetic species $[\mathbf{1}\text{–}\mathbf{8}]^{3+}$ systematically exhibit closely spaced rhombic or axial-type EPR spectra at 77 K corresponding to *g* values close to the free-electron value of 2.0023, thereby suggesting a radical complex formulation of $\{Ru^{II}(\mu\text{-}BL^{\cdot-})Ru^{II}\}$ instead of the usually expected alternative mixed-valence formulation of $\{Ru^{II}(\mu\text{-}BL^{2-})Ru^{III}\}$. Consequently, $[\mathbf{1}\text{–}\mathbf{7}]^{3+}$ display intense near-infrared transitions in the range 1200–1500 nm with a band width at half height ($\Delta\nu_{1/2}$) of 1900–3800 cm^{-1} which is lower than the calculated value of 3800–4600 cm^{-1} obtained using the Hush formula for a localized class II mixed-valence system. Electrogenerated EPR-inactive second-step oxidized species $[\mathbf{1}\text{–}\mathbf{8}]^{4+}$ have been described as spin-coupled radical-bridged mixed-valence ruthenium(II)(III) species, $\{Ru^{II}(\mu\text{-}BL^{\cdot-})Ru^{III}\}$. $[\mathbf{1}\text{–}\mathbf{8}]^{2+}$ exhibit multiple ligand-based reductions involving coordinated BL^{2-} as well as aap. The above preferential metal- or ligand-based accessible electron-transfer processes in the complexes have been further substantiated by DFT calculations on the geometry-optimized structure of $[\mathbf{1a}]^{2+}$.

Introduction

The design of newer classes of ligand-bridged polyruthenium systems in combination with selective ancillary ligands $[\{(AL)Ru\}_n(\mu\text{-}BL)]^{n+}$ (AL = ancillary ligand and BL = bridging ligand) has drawn special attention in recent years,[1] particularly from the perspective of tuning intermetallic electronic coupling processes in their mixed-valence states, which, in turn, finds partial applications in fabricating molecular electronic devices[2] as well as the theoretical understanding of electron-transfer processes.[3] A large number of polyruthenium derivatives have been studied and a wide variation of coupling aspects, including moderately coupled localized class II, strongly coupled delocalized class III, and hybrid or borderline class II–III situations[4,5] have emerged that primarily depend on the electronic states of the specific set of bridging and ancillary ligands. Although different kinds of molecular frameworks have been utilized as bridging ligands for assembling metal fragments in place, only a limited number of diruthenium complexes with the following redox-active polynucleating quinonoid bridging (BL) units along with selective ancillary ligands (AL) are known so far: 1,10-phenanthroline-5,6-dione (AL =

[a] Department of Chemistry, Indian Institute of Technology, Powai, Mumbai 400076, India
Fax: +91-22-2572-3480
E-mail: lahiri@chem.iitb.ac.in

Supporting information for this article is available on the WWW under http://www.eurjic.org or from the author.

acac$^-$[6]/bpy[7]), 1,10-phenanthroline-5,6-diimine (acac$^-$),[6] 2,5-dioxido-1,4-benzoquininediimines (bpy/acac$^-$),[8] 2,5-dioxido-1,4-benzoquinones (bpy),[9] 5,8-dioxido-1,4-naphthoquinone (bpy),[10] 1,4-dioxidoanthraquinone (bpy),[11] 1,5-dioxidoanthraquinone (bpy),[11] 1,2,4,5-tetraimino-3,6-diketocyclohexane (bpy),[12] 3,3′,4,4′-tetraoxybiphenyl (bpy),[13] 3,3′,4,4′-tetraiminobiphenyl (acac$^-$[14]/bpy[15]), and *p*-benzoquinonediimine(NH$_3$)[16] (bpy = 2,2′-bipyridine, acac$^-$ = acetylacetonate). The remarkable mixing of ruthenium and quinonoid frontier orbitals[17] is expected to facilitate the bridging-ligand-mediated intermetallic coupling processes in such systems; however, it also creates additional challenges in assigning the precise valence state combinations of the metal ion and the bridging ligand in the native state as well as towards the accessible electron-transfer processes. The extent of mixing of ruthenium- and quinonoid-based orbitals and their subsequent participation in the electron-transfer processes are also influenced by the involvement of the ancillary ligands (AL)[8,14,15] in the resultant molecular orbitals, and this is essentially the reason for the present program of developing larger quinonoid-bridged diruthenium complexes encompassing strongly π-accepting 2-arylazopyridine (aap) as ancillary ligands.

The present article thus describes the synthesis of a group of ten diruthenium complexes [(aap)$_2$Ru^{II}(μ-BL$_n^{2-}$)-Ru^{II}(aap)$_2$](ClO$_4$)$_2$ [**1a**–**1c**](ClO$_4$)$_2$ and [**2**–**8**](ClO$_4$)$_2$ {BL^{2-} = 5,8-dioxido-1,4-napthoquinone (BL$_1^{2-}$), 2,3-dichloro-5,8-dioxido-1,4-napthoquinone (BL$_2^{2-}$), 6,11-dioxido-5,12-naphthacenedione (BL$_3^{2-}$), 1,4-dioxido-9,10-anthraquinone(BL$_4^{2-}$), 2,3-dimethyl-1,4-dioxido-9,10-anthraquinone (BL$_5^{2-}$), 6,7-dichloro-1,4-dioxido-9,10-anthraquinone (BL$_6^{2-}$), 1,4-diimino-9,10-anthraquinone (BL$_7^{2-}$), and 1,5-dioxido-9,10-anthraquinone (BL$_8^{2-}$); aap = 2-arylazopyridine} and the crystal structures of two selected derivatives, namely [**1a**](ClO$_4$)$_2$ and [**3**](ClO$_4$)$_2$. The primary involvement of metal-, bridging-ligand-, or ancillary-ligand-based orbitals or a mixed situation in the accessible electron-transfer processes of the complexes has been scrutinized by UV/Vis/NIR spectroelectrochemistry and EPR investigations in combination with DFT/TDDFT calculations on the selected complex [**1a**]$^{2+}$. The specific effect of aap as an ancillary ligand in [**1**–**8**]$^{n+}$ with special reference to complexes with bpy[10,11] and BL$_1^{2-}$, BL$_4^{2-}$, and BL$_8^{2-}$ as bridging ligands are also highlighted.

Results and Discussion

Synthesis and Characterization

The present study deals with the eight quinonoid-based bridging ligands abbreviated as H$_2$BL$_{1-8}$. The bridging ligands differ in terms of their ring size (naphthaquinone- or anthraquinone-based frameworks), the substituents on the rings, and the positions of the donor centers in the rings. H$_2$BL$_7$ is the amine (NH$_2$) version of the hydroxy-containing H$_2$BL$_4$ (Scheme 1).

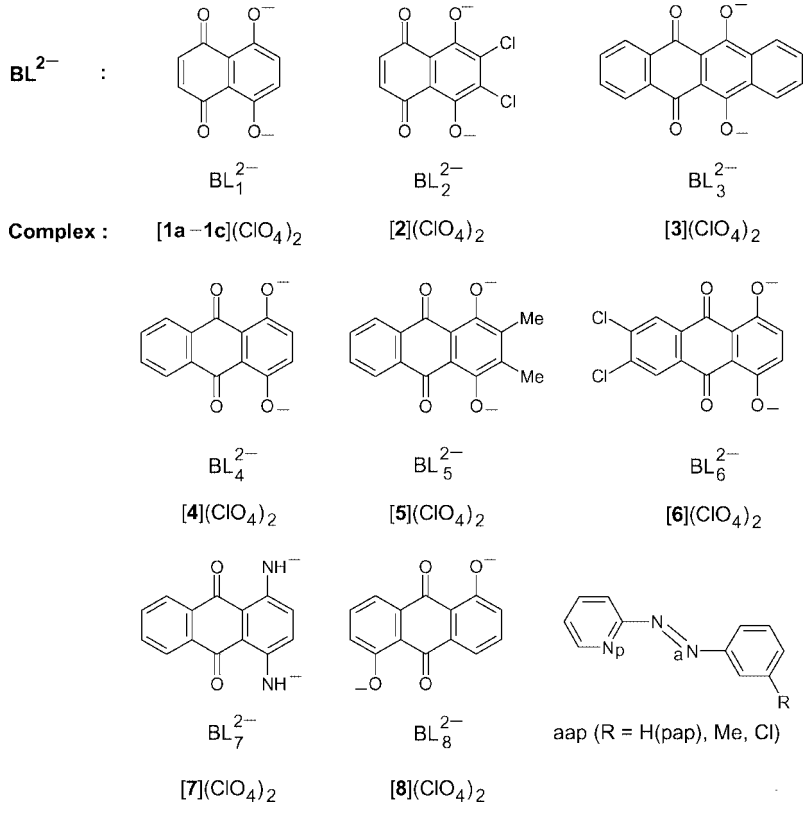

Scheme 1.

The complexes $[(pap)_2Ru^{II}(\mu\text{-}BL^{2-})Ru^{II}(pap)_2](ClO_4)_2$ {[**1a**]$(ClO_4)_2$ and [**2**–**8**]$(ClO_4)_2$; Scheme 1} were synthesized by following a general procedure involving treatment of the respective quinones (H_2BL) with an ethanolic solution of the metal precursor *ctc*-$[Ru^{II}(pap)_2(H_2O)_2](ClO_4)_2$ [pap = 2-phenylazopyridine; *ctc* = *cis*-*trans*-*cis* with respect to the aqua, pyridine (N_p), and azo (N_a) nitrogen atoms of pap, respectively} in the presence of sodium acetate as base under dinitrogen, followed by chromatographic purification on a neutral alumina column. The complexes [**1b**]$(ClO_4)_2$ and [**1c**]$(ClO_4)_2$ have 2-(*m*-tolylazo)pyridine and 2-(*m*-chlorophenylazo)pyridine, respectively, as ancillary ligands in combination with BL_1^{2-} (Scheme 1).

The *tc*-configuration [*tc* = *trans* and *cis* with respect to the pyridine (N_p) and azo (N_a) nitrogens, respectively] as well as the Ru^{II} state of the precursor metal fragment $\{Ru^{II}(pap)_2\}$ remain unaltered in complexes [**1**–**8**]$(ClO_4)_2$ (see below).

Although the reactions ideally lead to a mixture of *meso* ($\Delta\Lambda$) and *rac* ($\Delta\Delta/\Lambda\Lambda$) isomers,[18] the appearance of only one band, even on the preparatory TLC plate, in each case suggests either the presence of one particular diastereoisomeric form or an intimate mixture of *meso* and *rac* isomers in solution. The crystal structures of [**1a**]$(ClO_4)_2$ and [**3**]$(ClO_4)_2$ suggest the preferential crystallization of the *meso* isomer in both cases (see below).

The complexes are fairly soluble in polar (CH_3CN, DMF) as well as nonpolar (CH_2Cl_2) solvents. The diamagnetic (low-spin Ru^{II}, t_{2g}^6) complexes [**1**–**8**]$(ClO_4)_2$ are 1:2 conductors in CH_3CN and their microanalytical data (C,H,N) are in good agreement with the calculated values (see Exp. Sect.). The formation of the complexes was further confirmed by their electrospray mass spectroscopic data in CH_3CN (see Table 1 and Figure 1). The ^1H NMR spectra in $CDCl_3$ or $(CD_3)_2SO$ show partially overlapping signals corresponding to half of the molecule due to internal symmetry (see Figure 2 and Exp. Sect.). The closeness of the chemical shifts of the signals of several protons makes them appear as overlapping clusters. The ν(C=O) stretching frequency of the free H_2BL ligands (1616–1636 cm^{-1}) is absent in the IR spectra of the complexes, where a sharp peak appears in the range 1520–1582 cm^{-1}, thus indicating a delocalized keto-enol state of the coordinated bridging ligand BL^{2-}.[19] The delocalized keto-enol state of BL^{2-} is also clearly evidenced in the crystal structures of [**1a**]$(ClO_4)_2$ and [**3**]$(ClO_4)_2$ (see below). The ClO_4^- vibrations for all the complexes and the NH stretching fre-

Table 1. Mass spectroscopic data (*m*/*z*) in acetonitrile for [**1**–**8**]$(ClO_4)_2$.

Compound	Observed	Assignment	Calculated
[**1a**]$(ClO_4)_2$	1224.18	$[\{\mathbf{1a}\}ClO_4]^+$	1223.08
[**1b**]$(ClO_4)_2$	1279.14	$[\{\mathbf{1b}\}ClO_4]^+$	1279.14
[**1c**]$(ClO_4)_2$	1359.78	$[\{\mathbf{1c}\}ClO_4]^+$	1358.93
[**2**]$(ClO_4)_2$	1290.51	$[\{\mathbf{2}\}ClO_4]^+$	1291.01
[**3**]$(ClO_4)_2$	1322.97	$[\{\mathbf{3}\}ClO_4]^+$	1323.12
[**4**]$(ClO_4)_2$	1273.27	$[\{\mathbf{4}\}ClO_4]^+$	1273.10
[**5**]$(ClO_4)_2$	1301.41	$[\{\mathbf{5}\}ClO_4]^+$	1301.13
[**6**]$(ClO_4)_2$	1340.86	$[\{\mathbf{6}\}ClO_4]^+$	1341.02
[**7**]$(ClO_4)_2$	1270.95	$[\{\mathbf{7}\}ClO_4]^+$	1271.13
[**8**]$(ClO_4)_2$	1274.02	$[\{\mathbf{8}\}ClO_4]^+$	1273.10

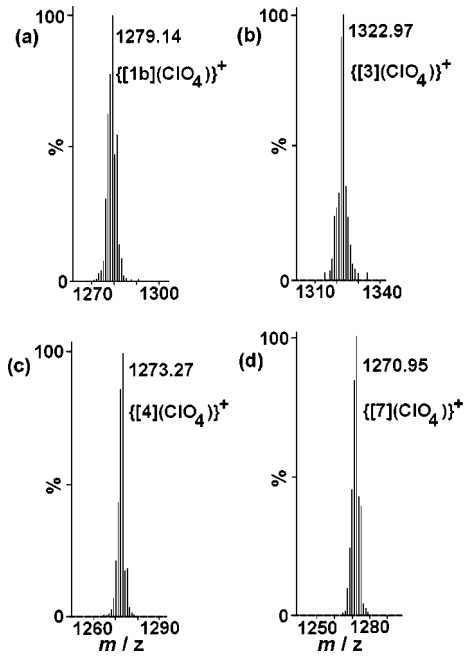

Figure 1. Mass spectra of [**1b**]$(ClO_4)_2$ (a), [**3**]$(ClO_4)_2$ (b), [**4**]$(ClO_4)_2$ (c), and [**7**]$(ClO_4)_2$ (d) in CH_3CN.

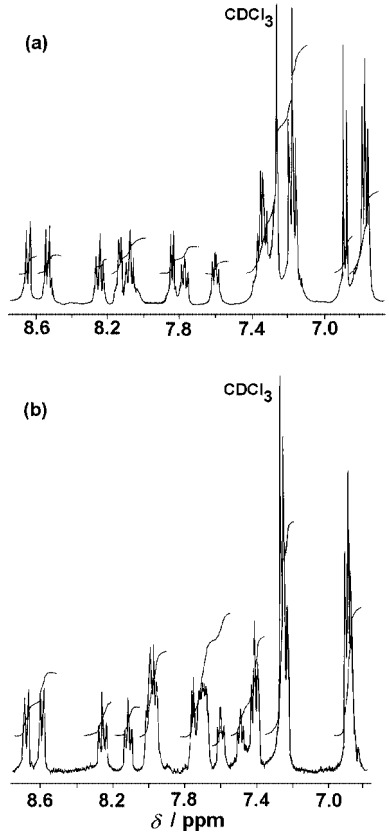

Figure 2. ^1H NMR spectra of [**1a**]$(ClO_4)_2$ (a) and [**3**]$(ClO_4)_2$ (b) in $CDCl_3$.

quency of the coordinated BL_7^{2-} in [**7**]$(ClO_4)_2$ appear in the expected positions of 1100/625 and 3260 cm^{-1}, respectively (see Exp. Sect.).

Crystal Structures of [1a]$(ClO_4)_2 \cdot H_2O$ and [3]$(ClO_4)_2$

The crystal structures of [**1a**]$(ClO_4)_2 \cdot H_2O$ and [**3**]$(ClO_4)_2$ are shown in Figures 3 and 4, respectively. Selected crystallographic parameters are given in the Exp. Sect. and bond lengths and angles are listed in Table 2. Both structures contain a crystallographic inversion center. Each Ru ion is bonded symmetrically to the dianionic bridging ligand BL^{2-} through the two oxygen donor centers at each end. The Ru centers are nearly coplanar with the bridging ligand; the angles between the planes consisting of the chelate ring containing the Ru ion to the bridging ligand and the planar bridging ligand are 1.57(0.71)° and 3.17(0.81)° for [**1a**]$(ClO_4)_2$ and [**3**]$(ClO_4)_2$, respectively. The RuO_2N_4 chromophore is in a distorted octahedral arrangement, as can be seen from the angles around the metal ion (Table 2). The two similar C–O distances in coordinated BL_1^{2-} [C2–O1/C4–O2 1.278(5)/1.291(4) Å] and BL_3^{2-} [C2–O1/C4–O2 1.282(7)/1.280(7) Å] and the corresponding intra-ring distances (Table 2) in [**1a**]$(ClO_4)_2$ and [**3**]$(ClO_4)_2$, respectively, signify the delocalized keto-enol state of the coordinated BL^{2-}.[19–21] The calculated (B3LYP/SDD, 6-31G* level of theory) bond lengths/angles and atomic charges of the dianionic form of free BL_1^{2-} (Figure 5 and Table 3; coordinates for the optimized BL_1^{2-} are given in Table S1 in the Supporting Information) also suggest its delocalized state. The Ru^{II}–O(BL^{2-}) distances [Ru1–O1/Ru1–O2 2.025(3)/2.038(3) and 2.009(4)/2.016(4) Å in [**1a**]$(ClO_4)_2$ and [**3**]$(ClO_4)_2$, respectively] agree well with known Ru^{II}–O (acetylacetonate, keto-enol delocalized form) distances.[21] The Ru–Ru separations in [**1a**]$(ClO_4)_2$ and [**3**]$(ClO_4)_2$ are 8.327 and 8.338 Å, respectively.

The {Ru(pap)$_2$} fragment is in a *tc*-configuration (*tc* = *trans* and *cis* with respect to the pyridine and azo nitrogens

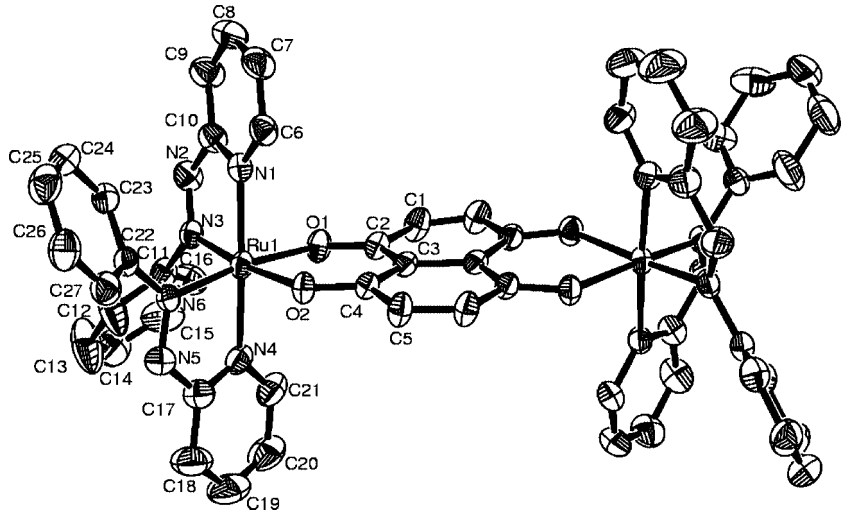

Figure 3. Crystal structure of the cation of [**1a**]$(ClO_4)_2$. Ellipsoids are drawn at 30% probability.

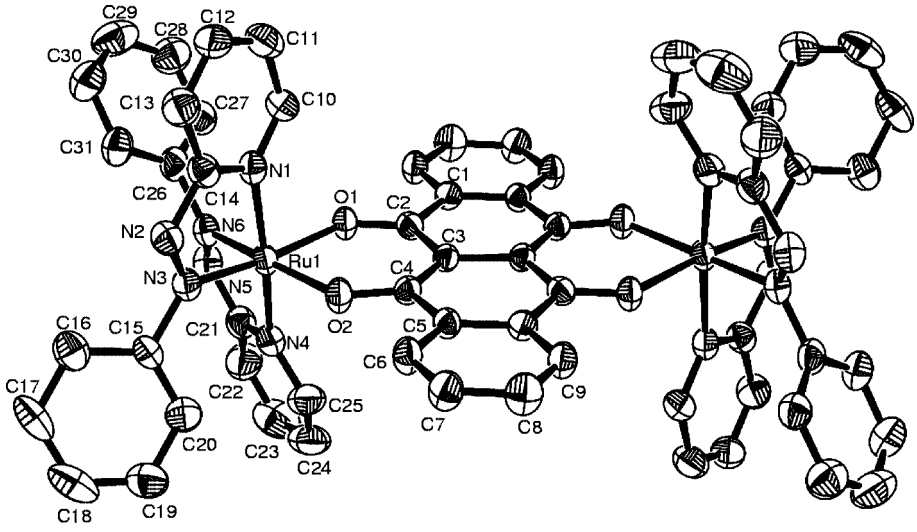

Figure 4. Crystal structure of the cation of [**3**]$(ClO_4)_2$. Ellipsoids are drawn at 30% probability.

Table 2. Experimental and calculated bond lengths [Å] and angles [°] for [**1a**]$(ClO_4)_2$ and [**3**]$(ClO_4)_2$.

	[**1a**]$(ClO_4)_2$ Exp.[a]	Comp.[b]	[**3**]$(ClO_4)_2$ Exp.		[**1a**]$(ClO_4)_2$ Exp.[a]	Comp.[b]	[**3**]$(ClO_4)_2$ Exp.
Ru(1)–N(1)	2.041(4)	2.071	2.030(6)	N(3)–Ru(1)–N(6)	98.53(14)	101.8	98.1(2)
Ru(1)–N(3)	1.957(3)	2.035	2.006(6)	N(3)–Ru(1)–O(1)	87.92(14)	86.3	169.1(2)
Ru(1)–N(4)	2.034(4)	2.071	2.058(6)	N(6)–Ru(1)–O(1)	170.97(12)	169.5	87.20(19)
Ru(1)–N(6)	2.018(3)	2.035	1.959(5)	N(3)–Ru(1)–N(4)	98.85(15)	102.7	106.5(2)
Ru(1)–O(1)	2.025(3)	2.059	2.009(4)	N(6)–Ru(1)–N(4)	76.86(15)	76.8	76.6(3)
Ru(1)–O(2)	2.038(3)	2.059	2.016(4)	O(1)–Ru(1)–N(4)	95.97(15)	94.9	83.9(2)
N(2)–N(3)	1.284(5)	1.286	1.298(7)	N(3)–Ru(1)–O(2)	172.99(13)	169.5	89.13(19)
N(5)–N(6)	1.288(5)	1.286	1.281(8)	N(6)–Ru(1)–O(2)	86.54(12)	86.3	171.8(2)
C(2)–O(1)	1.278(5)	1.289	1.282(7)	O(1)–Ru(1)–O(2)	87.61(12)	86.6	86.27(17)
C(4)–O(2)	1.291(4)	1.289	1.280(7)	N(4)–Ru(1)–O(2)	86.99(13)	85.7	97.8(2)
C(1)–C(2)	1.443(6)	1.450	1.457(9)	N(3)–Ru(1)–N(1)	77.21(14)	76.8	76.4(2)
C(2)–C(3)	1.426(5)	1.433	1.424(8)	N(6)–Ru(1)–N(1)	103.17(14)	102.7	94.8(2)
C(3)–C(4)	1.408(5)	1.433	1.412(8)	O(1)–Ru(1)–N(1)	84.36(13)	85.7	93.7(2)
C(4)–C(5)	1.438(6)	1.450	1.466(8)	N(4)–Ru(1)–N(1)	176.05(14)	179.2	171.2(2)
C(5)–C(6)	–	–	1.410(8)	O(2)–Ru(1)–N(1)	96.97(13)	94.9	90.5(2)
C(6)–C(7)	–	–	1.369(10)	O(1)–C(2)–C(3)	126.6(4)	126.9	126.3(6)
C(7)–C(8)	–	–	1.359(10)	C(3)–C(2)–C(1)	118.6(4)	118.6	120.1(6)
C(8)–C(9)	–	–	1.413(9)	C(4)–C(3)–C(2)	121.6(3)	120.8	120.6(5)
C(1)–C(1)#1	1.326(9)	1.351	–	O(2)–C(4)–C(3)	126.8(3)	129.9	126.0(5)
C(3)–C(3)#1	1.469(7)	1.464	1.452(11)	C(3)–C(4)–C(5)	118.8(3)	118.6	119.9(5)
C(5)–C(5)#1	1.327(8)	1.351	–				
C(1)–C(5)#1	–	–	1.383(8)				
C(5)–C(1)#1	–	–	1.383(8)				

[a] From X-ray crystal data. [b] Calculated at the B3LYP level of theory (see Exp. Sect.).

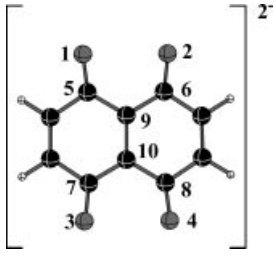

Figure 5. The B3LYP,6-31G*-optimized geometry for the singlet ground state of $[BL_1]^{2-}$.

Table 3. Selected geometrical parameters and atomic charges for the free BL_1^{2-} ligand optimized at the B3LYP/6-31G* level of theory.

Bond lengths [Å]		Bond and dihedral angles [°]	
O1–C5	1.262	O1–C5–C9	127.5
O2–C6	1.262	O2–C6–C9	127.5
O3–C7	1.262	O3–C7–C10	127.5
O4–C8	1.262	O4–C8–C10	127.5
C5–C9	1.459	O1–C5–C6–O2	0.00
C9–C6	1.459	O3–C7–C8–O4	0.00
C9–C10	1.474	O1–C5–C8–O4	180.0
C7–C10	1.459	O2–C6–C7–O3	180.0
C10–C8	1.459		
Atomic charges			
O1	–0.64	C5	0.34
O2	–0.64	C6	0.34
O3	–0.64	C7	0.34
O4	–0.64	C8	0.34

of pap, respectively), as is the case in the precursor complex.[22] The shortness of the Ru–N(azo) bonds [Ru1–N3 1.957(3) and 2.006(6), Ru1–N6 2.018(3) and1.959(5) Å for [**1a**]$(ClO_4)_2$ and [**3**]$(ClO_4)_2$, respectively] compared to the Ru–N(pyridine) bonds [Ru1–N1 2.041(4) and 2.030(6), Ru1–N4 2.034(4) and2.058(6) Å in [**1a**]$(ClO_4)_2$ and [**3**]$(ClO_4)_2$, respectively] reflects the π-back-bonding interaction $Ru^{II}(d\pi)\rightarrow pap(\pi*)$, where the pap(π*) level is predominantly azo in character.[23] A consequence of this is that the azo(N=N) distances of the coordinated pap ligand [N2–N3 1.284(5) and 1.297(7), N5–N6 1.288(5) and 1.281(8) Å in [**1a**]$(ClO_4)_2$ and [**3**]$(ClO_4)_2$, respectively] are significantly longer than that calculated (B3LYP,6-31G* level of theory) for the free pap ligand (1.259 Å, see Figure 6 and Table 4; coordinates for the optimized pap ligand are given in Table S2 in the Supporting Information), as is also the case in other reported complexes of arylazopyridine ligands.[24]

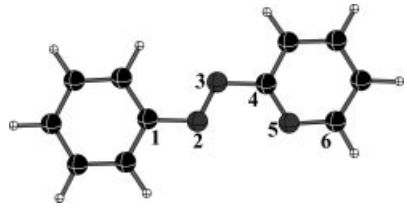

Figure 6. The B3LYP,6-31G*-optimized geometry for the singlet ground state of pap.

The optimized geometry of $[\mathbf{1a}]^{2+}$ is shown in Figure 7 and a selected list of optimized geometrical details of $[\mathbf{1a}]^{2+}$ is provided in Table 2 (coordinates and a full list of bond lengths and angles for the optimized $[\mathbf{1a}]^{2+}$ are provided in Tables S3 and S4, respectively, in the Supporting Information). In general, the computed structural details of $[\mathbf{1a}]^{2+}$ are in good agreement with the experimental param-

Table 4. Selected geometrical parameters and atomic charges of the free 2-(phenylazo)pyridine (pap) ligand obtained at the B3LYP/6-31G* level of theory.

Bond lengths [Å]		Bond and dihedral angles [°]	
C1–N2	1.419	C1–N2–N3	114.45
N2–N3	1.259	N2–N3–C4	114.86
N3–C4	1.425	N3–C4–N5	121.76
C4–N5	1.340	C4–N5–C6	117.21
N5–C6	1.333	C1–N2–N3–C4	179.27
		N2–N3–C4–N5	8.38
		N3–C4–N5–C6	179.55
Atomic charges			
C1	0.26	C4	0.46
N2	–0.26	N5	–0.43
N3	–0.31	C6	0.04

eters (Table 2). The calculated bond lengths of the coordinated BL_1^{2-} ligand in $[\mathbf{1a}]^{2+}$ also suggest its delocalized keto-enol nature.

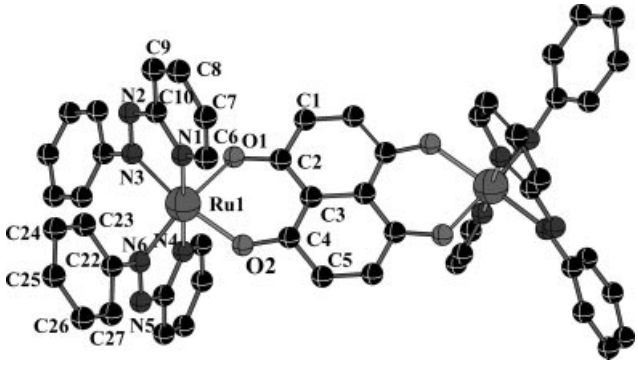

Figure 7. The B3LYP/SDD,6-31G*-optimized geometry for the singlet ground state of $[\mathbf{1a}]^{2+}$.

It should be noted that to the best of our knowledge $[\mathbf{1a}](ClO_4)_2$ and $[\mathbf{3}](ClO_4)_2$ are the first structurally characterized diruthenium complexes bridged by BL^{2-}, although the crystal structures of $[\{Co(tripod)\}_2(\mu\text{-}BL_1^{2-})]^{2+}$/$[\{Co(tripod)\}_2(\mu\text{-}BL_4^{2-})]^{2+}$ [tripod = $MeC(CH_2PPh_2)_3$],[25] $[\{Ph_4Sb\}_2(\mu\text{-}BL_1^{2-})]$,[26] $[Cu_2(dien)_2(\mu\text{-}BL_1^{2-})](BPh_4)_2$ (dien = diethylenetriamine),[27] $[\{Fe(salen)\}_2(\mu\text{-}BL_4^{2-})]$ [salen = *N*,*N*′-bis(salicylaldehyde)ethylenediimine],[28] and $[\{Rh(CO)(PPh_3)\}_2(\mu\text{-}BL_7^{2-})]$[29] have been reported.

Electrochemistry, EPR Spectroscopy, Spectrolectrochemistry, and Density Functional Calculations

Complexes $[\mathbf{1}–\mathbf{8}](ClO_4)_2$ exhibit two successive one-electron oxidation processes and multiple reductions in both CH_3CN and CH_2Cl_2 (Figure 8 and Table 5). The first oxidation potential of BL_1^{2-}-bridged $[\mathbf{1a}]^{2+}$–$[\mathbf{1c}]^{2+}$ varies slightly based on the electronic effect of the R group attached to the framework of the ancillary ligand (Scheme 1).[30]

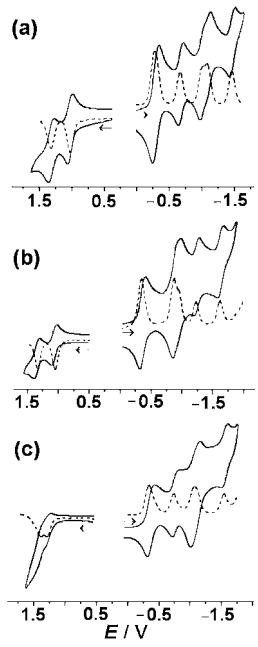

Figure 8. Cyclic voltammograms (—) and differential pulse voltammograms (----) of 10^{-3} M solutions of $[\mathbf{1a}](ClO_4)_2$ (a), $[\mathbf{4}](ClO_4)_2$ (b), and $[\mathbf{8}](ClO_4)_2$ (c) in CH_3CN/0.1 M Et_4NClO_4 at 298 K (scan rate: 50 mV s^{-1}).

The potentials of the complexes with pap in combination with different BL^{2-} ligands ($[\mathbf{1a}]^{2+}$ and $[\mathbf{2}]^{2+}$–$[\mathbf{8}]^{2+}$) vary substantially due to a variety of parameters associated with BL_n^{2-}, such as (i) the electronic nature of the substituents in BL_n^{2-}, (ii) the number of fused rings involved, (iii) the relative position of the oxygen donor centers in the anthracene ring (BL_4^{2-} and BL_8^{2-}), and (iv) the difference in donor centers in BL_4^{2-} (oxido) and BL_7^{2-} (iminium). The first oxidation potential follows the order $[\mathbf{8}]^{2+} >> [\mathbf{2}]^{2+} > [\mathbf{6}]^{2+} > [\mathbf{1a}]^{2+} \geq [\mathbf{4}]^{2+} > [\mathbf{3}]^{2+} > [\mathbf{5}]^{2+} >> [\mathbf{7}]^{2+}$ in both CH_3CN and CH_2Cl_2 (Table 5). The separation in potentials between the successive oxidation processes (ΔE) translates to the comproportionation constant K_c [derived from $RT\ln K_c = nF(\Delta E)$[31]], which has values in the range of 2.3×10^2–1.2×10^5 in CH_3CN (Table 5). The variation of the electronic nature of the substituents in the framework of the ancillary ligands (H, Me, Cl) with the same BL_1^{2-} bridging unit in $[\mathbf{1a}]^{2+}$–$[\mathbf{1c}]^{2+}$ has a small effect on the coupling processes. However, it is significantly large as in pap complexes $[\mathbf{1a}]^{2+}$ and $[\mathbf{2}]^{2+}$–$[\mathbf{8}]^{2+}$ with different BL_n^{2-} ligands. Complex $[\mathbf{8}]^{2+}$ shows the smallest electrochemical coupling (K_c) due to its larger Ru–Ru separation, which is a result of the spreading of donor centers (O,O,O,O) over all three available rings in the anthracene backbone unlike all other complexes ($[\mathbf{1}]^{2+}$–$[\mathbf{7}]^{2+}$), where only two consecutive fused rings are involved. The ΔE value, however, increases in CH_2Cl_2 in each case, leading to relatively higher K_c values of 1.7×10^3–1.3×10^6 (Table 5). The K_c values of the complexes are suggestive of an electrochemically moderately coupled, localized, class II mixed-valence situation.[32] The only other related diruthenium derivatives of large quinones (Scheme 1) with AL = bpy, namely $[\{(bpy)_2Ru\}_2(\mu\text{-}$

Table 5. Electrochemical data in acetonitrile (AN) and dichloromethane (DCM).

	Solv.	Oxidation couple $E°_{298}$ [V] (ΔE_p [mV])	ΔE [mV], K_c	Reduction couple $E°_{298}$ [V] (ΔE_p [mV])
$[\mathbf{1a}]^{2+}$	AN	1.06 (69), 1.36 (70)	300, 1.2×10^5	–0.30 (97),[a] –0.68 (72), –1.00 (62), –1.12 (64), –1.47 (75)
	DCM	1.13 (58), 1.46 (76)	330, 3.9×10^5	–0.33 (160),[a] –0.86 (118), –1.10 (96), –1.24 (92), –1.55 (126)
$[\mathbf{1b}]^{2+}$	AN	1.05 (61), 1.34 (60)	290, 8.2×10^4	–0.40 (65),[a] –0.85 (100),[a] –0.94 (80), –1.18 (90), –1.53 (93)
	DCM	1.11 (57), 1.43 (58)	320, 2.6×10^5	–0.22 (81), –0.61 (109), –0.78 (40), –1.18 (100), –1.68 (50)
$[\mathbf{1c}]^{2+}$	AN	1.09 (71), 1.40 (71)	310, 1.8×10^5	–0.26 (100),[a] –0.67 (53), –0.89 (120),[a] –1.48 (68)
	DCM	1.16 (90), 1.48 (50)	320, 2.6×10^5	–0.27 (110), 0.56 (30), –0.75 (40), –0.90 (50), –1.04 (80), –1.42 (80)
$[\mathbf{2}]^{2+}$	AN	1.14 (76), 1.41 (80)	270, 3.8×10^4	–0.36 (90),[a] –0.71 (66), –1.07 (60), –1.20 (62), –1.50 (61)
	DCM	1.20 (86), 1.52 (68)	320, 2.6×10^5	–0.29 (89),[a] –0.82 (40), –1.19 (60), –1.48 (40)
$[\mathbf{3}]^{2+}$	AN	0.99 (79), 1.25 (80)	260, 2.5×10^4	–0.40 (59),[a] –0.94 (66),[a] –1.43 (60), –1.76 (73)
	DCM	1.10 (72), 1.38 (60)	280, 5.5×10^4	–0.31 (130),[a] –0.99 (62),[a] –1.42 (42), –1.76 (93)
$[\mathbf{4}]^{2+}$	AN	1.04 (79), 1.33 (79)	290, 8.2×10^4	–0.38 (95),[a] –0.88 (120),[a] –0.97 (68), –1.24 (79), –1.63 (78)
	DCM	1.13 (168), 1.47 (162)	340, 5.7×10^5	–0.33 (110),[a] –0.96 (55), –1.14 (150), –1.49 (170), –1.85 (150)
$[\mathbf{5}]^{2+}$	AN	0.98 (59), 1.28 (69)	300, 1.2×10^5	–0.40 (81), –0.93 (120),[a] –1.37 (67), –1.76 (63)
	DCM	1.05 (121), 1.41 (142)	360, 1.3×10^6	–0.35 (130),[a] –0.98 (120), –1.15 (140), –1.51 (180), –1.84 (170)
$[\mathbf{6}]^{2+}$	AN	1.08 (74), 1.36 (86)	280, 5.6×10^4	–0.37 (120),[a] –0.90 (126),[a] –1.57 (74), –1.95 (60)
	DCM	1.17 (131), 1.52 (110)	350, 8.5×10^5	–0.30 (144),[a] –1.00 (140),[a] –1.37 (160), –1.70 (180)
$[\mathbf{7}]^{2+}$	AN	0.54 (95), 0.84 (76)	300, 1.2×10^5	–0.47 (96),[a] –0.80 (46), –1.04 (72),[a] –1.64 (80), –1.90 (67)
	DCM	0.60 (115), 0.93 (105)	330, 4.0×10^5	–0.42 (180),[a] –0.95 (140), –1.13 (120), –1.68 (160)
$[\mathbf{8}]^{2+}$	AN	1.26 (34), 1.40 (74)	140, 2.3×10^2	–0.36 (80),[a] –0.75 (65), –1.05 (43),[a] –1.56 (57)
	DCM	1.36 (77), 1.55 (54)	190, 1.7×10^3	–0.31 (151),[a] –0.88 (100), –1.16 (170), –1.41 (110), –1.58 (60)

[a] Two-electron transfer process.

$BL_1^{2-})]^{2+}$,[10] $[\{(bpy)_2Ru\}_2(\mu\text{-}BL_4^{2-})]^{2+}$,[11] and $[\{(bpy)_2Ru\}_2(\mu\text{-}BL_8^{2-})]^{2+}$,[11] exhibit K_c values of 1.8×10^5, 3.7×10^4 and 3.4×10^2, respectively, in CH_3CN, similar to those of the corresponding pap complexes $[\mathbf{1}]^{2+}$, $[\mathbf{4}]^{2+}$, and $[\mathbf{8}]^{2+}$ (Table 5) in spite of the much stronger π-acceptor characteristics of pap relative to bpy.[33]

Both the metal ion and the bridging ligand in $[\mathbf{1}]^{2+}$–$[\mathbf{8}]^{2+}$ (Scheme 2) are able to undergo successive two-step one-electron oxidations with formation of paramagnetic intermediate species. Therefore, the preferential involvement of metal- or ligand-based frontier orbitals in the first oxidation process was ascertained from the EPR characteris-

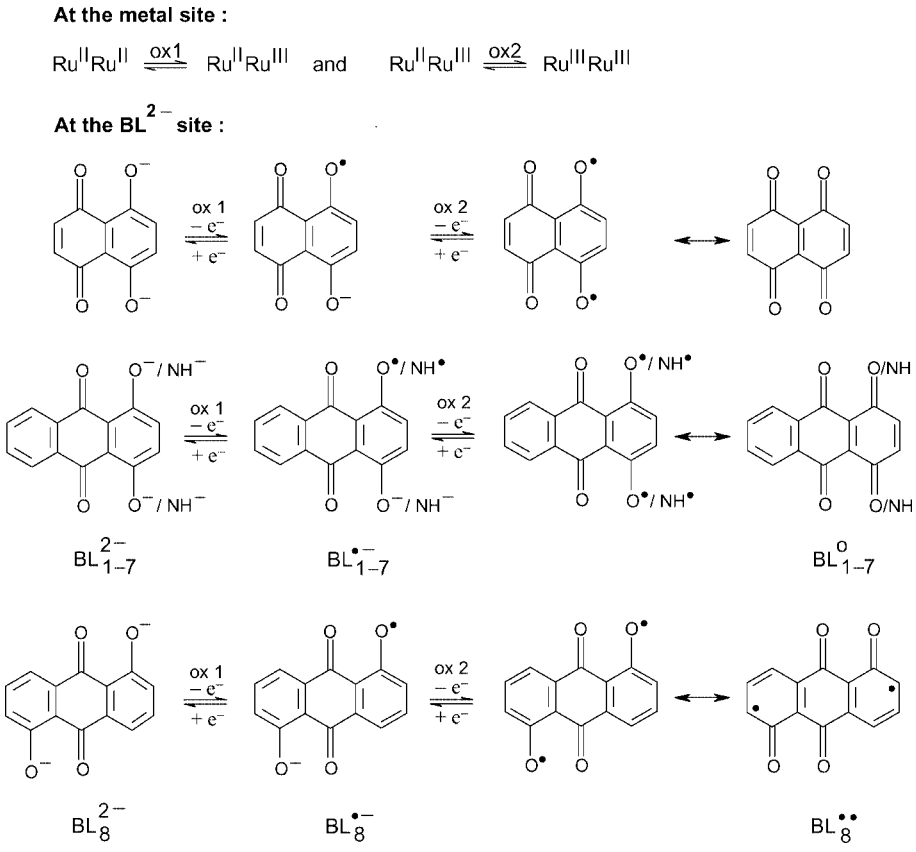

Scheme 2.

tics of the electrogenerated one-electron oxidized species in each case. The intermediate paramagnetic species $[\mathbf{1}–\mathbf{8}]^{3+}$ systematically exhibit closely spaced rhombic or axial-type EPR spectra at 77 K (Figure 9 and Table 6). However, analysis of the EPR spectra, especially the small g anisotropy ($\Delta g = g_1 - g_3 = 0.0078–0.0642$) and the average g $\{<g> = [(g_1^2 + g_2^2 + g_3^2)/3]^{1/2} \approx 2.00\}$,[34] which is close to the free electron value of 2.0023, clearly suggest a radical complex[35] with the formulation $Ru^{II}(\mu\text{-}BL^{\cdot-})Ru^{II}$ for $[\mathbf{1}–\mathbf{8}]^{3+}$ instead of the mixed-valence alternative $Ru^{II}(\mu\text{-}BL^{2-})Ru^{III}$. However, the observed small splitting of the EPR spectra implies a minority contribution of a paramagnetic Ru^{III} ion in the singly occupied molecular orbital (SOMO) as well, which leads to the alternative mixed-valence formulation $Ru^{II}(\mu\text{-}BL^{2-})Ru^{III}$.[36] The appreciable effect of the electronic structure of BL^{2-} on the first oxidation potential of $[\mathbf{1}–\mathbf{8}]^{2+}$ (Table 5) indeed justifies its preferential involvement. The above assignments are in good agreement with the computed HOMO energies of $[\mathbf{1a}]^{2+}$ at the B3LYP level (Figure 10 and Table 7). The contribution of 68% $\pi(BL_1^{2-})$ along with 22% $d\pi(Ru)$ in the HOMO level essentially justifies the preferential primary involvement of BL_1^{2-} instead of Ru^{II} in the first oxidized state, as clearly evidenced in the EPR spectra of $[\mathbf{1}–\mathbf{8}]^{3+}$. The intermediate one-electron oxidized species for the analogous bpy complexes $[\{(bpy)_2Ru\}_2(\mu\text{-}BL_1^{2-})]^{3+}$,[10] $[\{(bpy)_2Ru\}_2(\mu\text{-}BL_4^{2-})]^{3+}$,[11] and $[\{(bpy)_2Ru\}_2(\mu\text{-}BL_8^{2-})]^{3+}$[11] were, however, ascribed to a mixed-valence $Ru^{II}Ru^{III}$ situation based on the EPR spectrum of the isolated polycrystalline $[\{(bpy)_2Ru\}_2(\mu\text{-}BL_1^{2-})]^{3+}$ at 77 K ($g_1 = 2.33$, $g_2 = 2.01$, and $g_3 = 1.88$; $\Delta g = 0.45$ and $<g> = 2.08$) and the near-IR transition at 2083 nm in CH_3CN ($\varepsilon = 9120\ M^{-1}cm^{-1}$, $\Delta\nu_{1/2} = 3000\ cm^{-1}$). The preferential involvement of the bridging ligand in the first oxidation process has been described recently in the smaller quinonoid-based diruthenium(II)-bpy complex $[\{(bpy)_2Ru^{II}\}_2(\mu\text{-}H_2L^{2-})]^{2+}$ (H_2L^{2-} = 2,5-dioxido-1,4-benzoquinonediimine).[7] However, the K_c value for the successive oxidation processes in $[\{(bpy)_2Ru^{II}\}_2(\mu\text{-}H_2L^{2-})]^{2+}$ is much higher (6.5×10^8 in CH_3CN) than that in the present cases (ca. 10^2–10^5), as normally expected for ligand-based processes.[14,36]

Electrochemically generated further one-electron oxidized species $[\mathbf{1}–\mathbf{8}]^{4+}$ are found to be EPR inactive even when frozen in a glass (77 K). The diamagnetic nature of the doubly oxidized species $[\mathbf{1}–\mathbf{8}]^{4+}$ suggests their probable alternative formulation as $\{Ru^{II}(\mu\text{-}BL^{\circ})Ru^{II}\}$, with involvement of the bridging ligand in the second step oxidation process, or $\{Ru^{II}(\mu\text{-}BL^{\cdot-})Ru^{III}\}$, with involvement of the metal ion in the second step oxidation process and subsequent antiferromagnetic spin pairing of the unpaired electrons associated with $BL^{\cdot-}$ and Ru^{III}. The computed orbital compositions in $[\mathbf{1a}]^{2+}$ at the B3LYP level suggest that the HOMO–1 and HOMO–2 are primarily dominated by Ru (61% and 70%, respectively), with only a minor contribution (ca. 10%) from BL_1^{2-} (Figure 10 and Table 7), which rules out the alternative possibility of a bridging-ligand-based second oxidation process. It should be noted that the stabilization of alternative spin-coupled singlet states by the involvement of a mixed-valence $Ru^{II}Ru^{III}$ configuration and an azo anion radical-based bridging ligand in $[(acac)_2Ru^{II}(\mu\text{-}L^{\cdot-})Ru^{III}(acac)_2]$ $\{L^{\cdot-} = NC_5H_4(N{=}N^{\cdot-})H_4C_5N\}$[18a] or partially coupled semiquinone form of 1,10-phenanthroline-5,6-dione ($L_1^{\cdot-}$) bridged $[(acac)_2Ru^{II}(\mu\text{-}L_1^{\cdot-})Ru^{III}(acac)_2]$ (acac = acetylacetonate) has been reported recently.[6] The consideration of a ruthenium-based second-step oxidation process ($Ru^{II}\rightarrow Ru^{III}$) instead of further oxidation of $BL^{\cdot-}$ can easily be understood, particularly in the case of $[\mathbf{8}]^{4+}$, as the alternative option leads to the formation of an unstable diradical-bridged triplet species $Ru^{II}(\mu\text{-}BL_8^{\cdot\cdot})Ru^{II}$ (Scheme 2). It is interesting to note that the occupied frontier orbitals (HOMO to HOMO–2) exhibit a fairly good mixing with the π orbitals of pap in $[\mathbf{1a}]^{2+}$ (Figure 10 and Table 7).

The formulations of analogous two-electron-oxidized bpy complexes $[\{(bpy)_2Ru\}_2(\mu\text{-}BL_1)]^{4+}$[10] and $[\{(bpy)_2Ru\}_2(\mu\text{-}BL_4)]^{4+}/[\{(bpy)_2Ru\}_2(\mu\text{-}BL_8)]^{4+}$ [11] were, on the other hand, proposed as $\{Ru^{II}(\mu\text{-}BL_1^{\circ})Ru^{II}\}$ and $\{Ru^{III}(\mu\text{-}BL_{4/8}^{2-})Ru^{III}\}$, respectively.

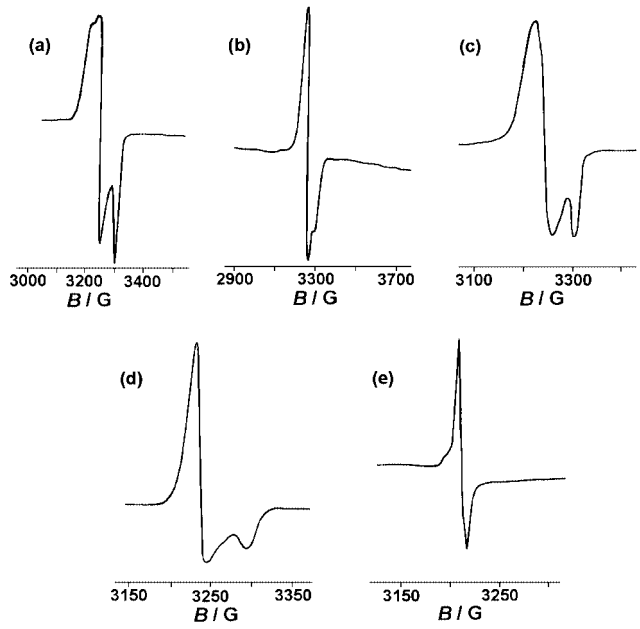

Figure 9. EPR spectra of $[\mathbf{1a}]^{3+}$ (a), $[\mathbf{3}]^{3+}$ (b), $[\mathbf{4}]^{3+}$ (c), $[\mathbf{7}]^{3+}$ (d), and $[\mathbf{8}]^{3+}$ (e) in CH_3CN/Et_4NClO_4 at 77 K.

Table 6. EPR data of electrogenerated $[\mathbf{1}–\mathbf{8}]^{3+}$ in acetonitrile at 77 K.

Compd.	g_1	g_2	g_3	Δg[a]	$<g>$[b]
$[\mathbf{1a}]^{3+}$	2.0242	2.0023	1.9659	0.0583	1.9976
$[\mathbf{1b}]^{3+}$	2.0273	2.0023	1.9630	0.0642	1.9977
$[\mathbf{1c}]^{3+}$	2.0273	2.0023	1.9660	0.0613	1.9987
$[\mathbf{2}]^{3+}$	2.0254	1.9992	1.9629	0.0625	1.9960
$[\mathbf{3}]^{3+}$	2.0085	2.0023	1.9737	0.0348	1.9949
$[\mathbf{4}]^{3+}$	2.0147	2.0023	1.9648	0.0499	1.9940
$[\mathbf{5}]^{3+}$	2.0146	2.0047	1.9661	0.0485	1.9952
$[\mathbf{6}]^{3+}$	2.0211	2.0035	1.9628	0.0583	2.0064
$[\mathbf{7}]^{3+}$	2.0057	2.0026	1.9661	0.0396	1.9915
$[\mathbf{8}]^{3+}$	2.0054	2.0023	1.9976	0.0078	2.0018

[a] $\Delta g = g_1 - g_3$. [b] $<g> = [(g_1^2 + g_2^2 + g_3^2)/3]^{1/2}$.

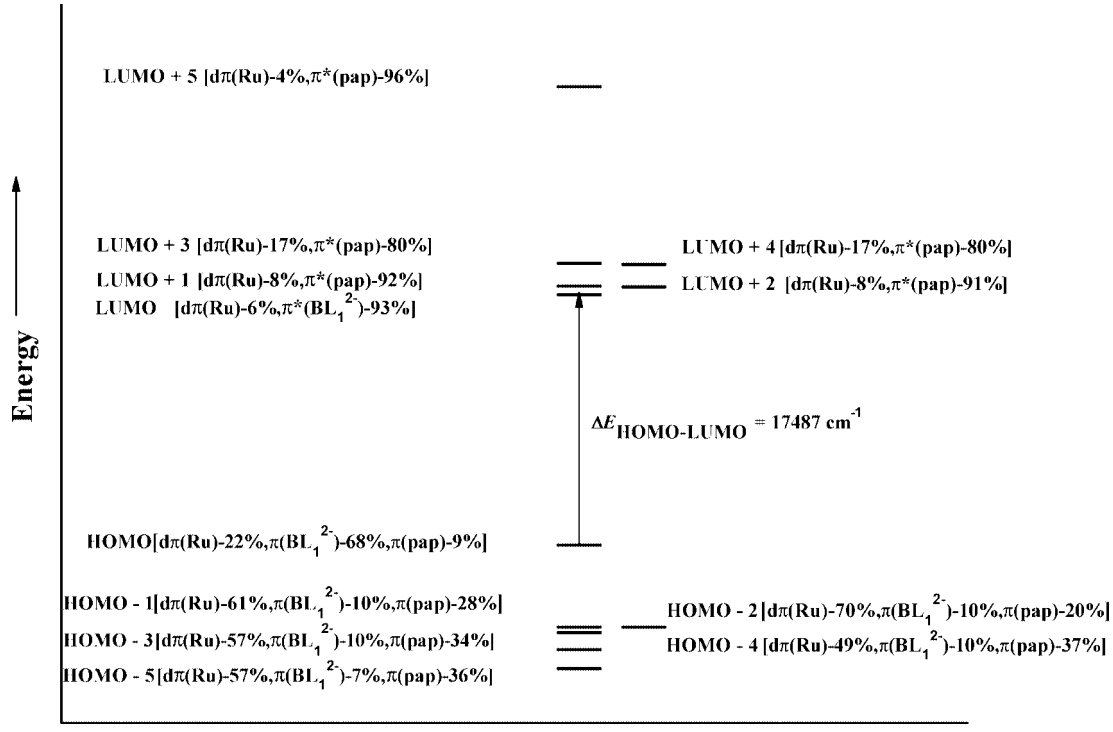

Figure 10. Orbital energy diagram for $[\mathbf{1a}]^{2+}$ computed at the B3LYP/SDD,6-31G* level of theory.

Table 7. Orbital energies and percent contributions of frontier molecular orbitals of $[\mathbf{1a}]^{2+}$ computed at the B3LYP level of theory by employing the SDD basis set for Ru and 6-31G* for all other atoms.

	Ru center	Bridging ligand (BL_1^{2-})	Ancillary ligand (pap)
LUMO+5 (–0.197)[a]	3.6	–	96.0
LUMO+4 (–0.254)	17.0	2.3	80.0
LUMO+3 (–0.254)	17.0	1.7	80.0
LUMO+2 (–0.263)	8.2	1.2	90.8
LUMO+1 (–0.263)	8.0	0.6	92.0
LUMO (–0.265)	6.2	92.9	–
HOMO (–0.346)	2.4	68.5	9.2
HOMO–1 (–0.373)	61.4	10.3	28.4
HOMO–2 (–0.373)	70.0	9.7	20.0
HOMO–3 (–0.374)	56.6	9.8	33.6
HOMO–4 (–0.380)	48.8	10.1	37.2
HOMO–5 (–0.387)	56.8	7.0	36.0

[a] Values in parentheses are orbital energies in atomic units.

Both the ancillary (aap)[37] and bridging ligand (BL^{2-})[10,11] are known to successively accept two electrons each in their LUMOs (Scheme 3), therefore ideally a total of ten one-electron reduction processes (eight from four aap ligands and two from BL^{2-}) are expected for $[\mathbf{1}–\mathbf{8}]^{2+}$. The complexes indeed display multiple reductions in CH_3CN or CH_2Cl_2 (Figure 8 and Table 5) within the accessible potential limit of –2.0 V. However, instead of ten successive one-electron reduction processes, simultaneous two-electron processes are also detected along with the clear one-electron responses, as confirmed by comparing the current heights of their respective DPVs (differential pulse voltammograms) with that of the coulometrically established one-electron oxidation processes. Since the ruthenium ion in $[\mathbf{1}–\mathbf{8}]^{2+}$ is in the +2 state, aap and BL^{2-} ligands are naturally involved in the reduction processes. Consequently, the reduction potentials vary systematically depending on the electronic structures of both aap and BL^{2-} (Table 5). The two-electron nature of the first reduction process for most of the complexes does not permit the radical intermediate to be electrogenerated (Scheme 3). However, the first one-electron reduced species for $[\mathbf{5}]^{+}$ in CH_3CN displays a free radical EPR signal at 77 K with $g = 1.998$ (Figure 11) without any hyperfine splitting, which might suggest that the unpaired electron resides on the oxygen center of $BL_5^{\cdot 3-}$ instead of the nitrogen center of the azo group of pap.[35,38] The B3LYP/6-31G* Kohn–Sham orbitals show that the LUMO is primarily dominated by the π* orbital of BL_1^{2-} (93%) whereas LUMO+1/LUMO+2 consist of π* orbitals of pap (>90%; Figure 10 and Table 7). The closeness in energy between the BL_1^{2-}-based LUMO and the pap-based higher vacant orbitals (LUMO+1/LUMO+2) justifies the observed simultaneous two-electron first step reduction process (Figure 8).

The spectral features of the complexes both in the native state $[\mathbf{1}–\mathbf{8}]^{2+}$ and also in the oxidized $[\mathbf{1}–\mathbf{8}]^{3+}/[\mathbf{1}–\mathbf{8}]^{4+}$ states follow a general trend in CH_3CN (Figure 12 and Table 8). The spectral features of $[\mathbf{1a}–\mathbf{1c}]^{n+}$ (n = 2, 3, 4) in CH_2Cl_2 also show a similar general trend and no significant solvent effect on the spectral aspects is observed. Multiple ligand-based π–π*/n–π* transitions appear in the UV region. In addition, intense metal-to-ligand charge transfer (MLCT) transitions are observed near 550 nm, which are associated with a moderately intense shoulder(s) at the lower energy part near 650 nm. The Gaussian analysis of the visible region part of the spectra of $[\mathbf{1a}]^{2+}$ in CH_3CN and CH_2Cl_2

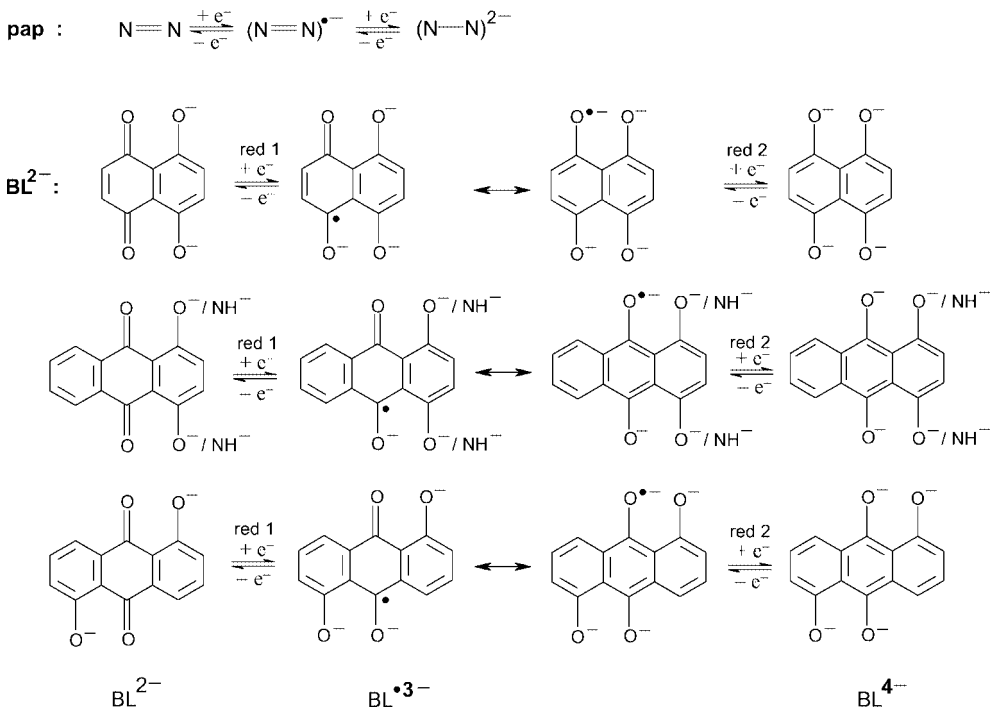

Scheme 3.

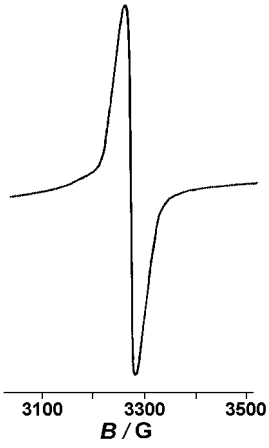

Figure 11. EPR spectrum of $[5]^+$ in CH_3CN/Et_4NClO_4 at 77 K.

shows a total of four bands at λ (ε) = 742 nm (4396 $M^{-1}cm^{-1}$), 639 (5580), 565 (11821), and 517 (22069) (see part a in Figure 12, inset) and 748 (4800), 656 (5739), 570 (11120), and 522 (23527) (Figure 12, part b, inset), respectively. A selected list of vertical excitation energies computed with the TD-DFT/B3LYP formalism for the B3LYP/SDD,6-31G* geometry of $[\mathbf{1a}]^{2+}$ in its singlet ground state are summarized in Table 9 (complete lists are given in Table S5 in the Supporting Information).[39] Here, a comparison between observed and computed transitions is performed by examining transitions of comparable intensities guided by their respective oscillator strengths and absorptivity values.[40] The nature of the excited states is assigned based on the percent Kohn–Sham orbital contributions of the orbitals involved in the electronic transitions. Based on the oscillator strengths, the comparable predicted transitions appear at λ = 743.91 (HOMO→LUMO+1), 696.64 (HOMO→LUMO/HOMO→LUMO+4), 539.14 (HOMO–2→LUMO/HOMO–1→LUMO+2) and 514.30 nm (HOMO–5→LUMO+1/HOMO–4→LUMO+2) (Table 9, Figure 13, and Figure S1 in the Supporting Information).

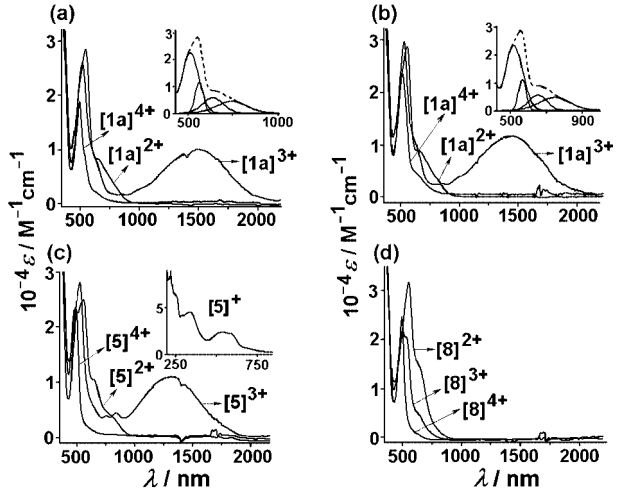

Figure 12. Electronic spectra of (a) $[\mathbf{1a}]^{n+}$ (n = 2–4) in CH_3CN/Et_4NClO_4. The inset shows the Gaussian analysis of the visible region of the spectrum for n = 2. (b) $[\mathbf{1a}]^{n+}$ (n = 2–4) in CH_2Cl_2/Et_4NClO_4. The inset shows the Gaussian analysis of the visible region of the spectrum for n = 2. (c) $[\mathbf{5}]^{n+}$ (n = 2–4) in CH_3CN/Et_4NClO_4. The inset shows the spectrum of $[\mathbf{5}]^+$. (d) $[\mathbf{8}]^{n+}$ (n = 2, 3, 4) in CH_3CN/Et_4NClO_4.

The charge-transfer bands of $[\mathbf{1}–\mathbf{8}]^{3+}$ are blue shifted upon oxidation, with a reduction in intensity, and a new low-energy, intense transition appears in the range 1200–

Table 8. Spectroelectrochemical data for $[\mathbf{1a}]^{n+}$–$[\mathbf{1c}]^{n+}$ in dichloromethane (DCM) and $[\mathbf{1}]^{n+}$–$[\mathbf{8}]^{n+}$ in acetonitrile (AN) (n = 2–4).

	Solvent	λ_{max} [nm] (ε [$M^{-1}cm^{-1}$])
$[\mathbf{1a}]^{2+}$	AN	669 (8260, sh), 554 (28300), 503 (22100, sh), 332 (35900), 286 (31200, sh)
	DCM	666 (8910, sh), 561 (28800), 505 (22400, sh), 344 (38400), 288 (31900, sh)
$[\mathbf{1a}]^{3+}$	AN	1500 (9960, 3007,[a] 3924[b]), 623 (9120, sh), 526 (25870), 502 (23400, sh), 363 (37100), 313 (33300, sh), 283 (37000)
	DCM	1439 (11600, 3246,[a] 4006[b]), 645 (9590, sh), 534 (29700), 496 (21900, sh), 367 (39500), 313 (33600, sh), 287 (36300)
$[\mathbf{1a}]^{4+}$	AN	550 (8540, sh), 502 (18800), 471 (12300, sh), 363 (34800), 310 (30300, sh), 282 (34500)
	DCM	641 (4510, sh), 519 (23500), 485 (16100, sh), 367 (43900), 308 (39700, sh), 287 (41600)
$[\mathbf{1b}]^{2+}$	AN	668 (10300, sh), 551 (32600), 507 (27100, sh), 346 (52300), 280 (35300)
	DCM	661 (7620, sh), 556 (22400), 504 (17900, sh), 356 (30900), 284 (24000)
$[\mathbf{1b}]^{3+}$	AN	1482 (8400, 3156,[a] 3948[b]), 613 (9500, sh), 520 (22000), 470 (14200, sh), 370 (35900), 355 (34100, sh), 283 (33700)
	DCM	1484 (8930, 3104,[a] 3945[b]), 638 (8630, sh), 535 (22000), 497 (16500, sh), 374 (31300), 314 (24100, sh), 284 (27100)
$[\mathbf{1b}]^{4+}$	AN	548 (9460, sh), 501 (21400), 471 (15100, sh), 370 (43300), 311 (33700, sh), 280 (40800)
	DCM	624 (9500, sh), 517 (23800), 490 (19800, sh), 371 (42400), 310 (45700, sh), 285 (44600)
$[\mathbf{1c}]^{2+}$	AN	666 (10400 sh), 541 (31800), 505 (27400, sh), 323 (46800), 284 (41000, sh)
	DCM	689 (8930, sh), 549 (26200), 514 (23800, sh), 336 (40100), 284 (32800, sh)
$[\mathbf{1c}]^{3+}$	AN	1416 (8880, 3130,[a] 4039[b]), 629 (8670, sh), 520 (27200), 470 (17300, sh), 351 (46400), 308 (43600, sh), 284 (45200)
	DCM	1405 (11000, 3387,[a] 4054[b]), 641 (10200, sh), 537 (28900), 495 (20800, sh), 356 (40700), 284 (37400)
$[\mathbf{1c}]^{4+}$	AN	545 (11100, sh), 504 (28400), 470 (18500, sh), 346 (52300), 310 (49300, sh), 280 (54400)
	DCM	636 (5050, sh), 522 (23800), 493 (18900, sh), 349 (46600), 284 (44800)
$[\mathbf{2}]^{2+}$	AN	655 (9280, sh), 553 (32400), 496 (22600, sh), 329 (38600), 285 (32500, sh)
$[\mathbf{2}]^{3+}$		1530 (10100, 3063,[a] 3885[b]), 642 (8490, sh), 527 (26000), 481 (17800, sh), 362 (35400), 309 (33600, sh), 284 (35900)
$[\mathbf{2}]^{4+}$		524 (9680, sh), 501 (22200), 362 (41300), 472 (14800, s), 306 (35400, sh), 280 (44900)
$[\mathbf{3}]^{2+}$	AN	802 (4250, sh), 618 (12500, sh), 569 (25100), 531 (20800, sh), 480 (19600), 370 (39000, sh), 335 (42300), 275 (70700)
$[\mathbf{3}]^{3+}$		1286 (9200, 3810,[a] 4238[b]), 623 (6510, sh), 534 (23600), 499 (21200, sh), 365 (38200), 275 (66800)
$[\mathbf{3}]^{4+}$		556 (5630, sh), 501 (20800), 476 (15000, sh), 362 (44600), 309 (35900, sh), 280 (44400)
$[\mathbf{4}]^{2+}$	AN	807 (2920, sh), 666 (8620, sh), 558 (23000), 488 (20300, sh), 335 (36200), 283 (34800)
$[\mathbf{4}]^{3+}$		1381 (5720, 3522,[a] 4090[b]), 612 (4450, sh), 530 (15100), 501 (13200, sh), 360 (20200), 310 (19400, sh), 283 (21800)
$[\mathbf{4}]^{4+}$		542 (3280, sh), 501 (12200), 475 (8620, sh), 361 (24300), 307 (19300, sh), 280 (22700)
$[\mathbf{5}]^{+}$	AN	706 (6160, sh), 597 (22200), 530 (23800), 341 (45100), 293 (41900, sh), 246 (65500, sh)
$[\mathbf{5}]^{2+}$		792 (4270, sh), 657 (10500, sh), 561 (25100), 488 (23500, sh), 336 (42900), 268 (59400)
$[\mathbf{5}]^{3+}$		1320 (10900, 3608,[a] 4183[b]), 648 (5710, sh), 534 (28100), 503 (25100, sh), 362 (38800), 283 (42200, sh), 265 (59400)
$[\mathbf{5}]^{4+}$		519 (14900, sh), 500 (22900), 472 (15900, sh), 358 (46100), 306 (35000, sh), 278 (43800)
$[\mathbf{6}]^{2+}$	AN	662 (8210, sh), 550 (22500), 493 (19300, sh), 329 (34000), 274 (44000)
$[\mathbf{6}]^{3+}$		1416 (8220, 3677 ,[a] 4039[b]), 622 (6930, sh), 528 (21100), 506 (20100, sh), 363 (30500), 282 (39600)
$[\mathbf{6}]^{4+}$		530 (5750, sh), 501 (17500), 473 (12400, sh), 361 (87100), 306 (27100, sh), 279 (35500)
$[\mathbf{7}]^{2+}$	AN	943 (4310, sh), 664 (6260, sh), 550 (20500), 491 (21500), 349 (38800), 304 (40700), 237 (60400, sh)
$[\mathbf{7}]^{3+}$		1274 (7170, 1913,[a] 4258[b]), 911 (8870, sh), 539 (21100, sh), 504 (24800), 373 (36700), 317 (31900, sh), 228 (54400, sh)
$[\mathbf{7}]^{4+}$		892 (21100), 499 (26100), 370 (39000), 282 (34300, sh), 234 (48500, sh)
$[\mathbf{8}]^{2+}$	AN	653 (14400, sh), 561 (31700), 487 (18800, sh), 360 (40500, sh), 319 (44700), 250 (61600, sh), 225 (85900)
$[\mathbf{8}]^{3+}$		638 (4960, sh), 546 (20300, sh), 508 (21500), 472 (16000, sh), 356 (44800), 308 (45000), 284 (42700, sh)
$[\mathbf{8}]^{4+}$		501 (24800), 475 (17600, sh), 363 (44800), 307 (36600, sh), 280 (45400)

[a] Experimental band width at half height ($\Delta\nu_{1/2}$). [b] Calculated band width at half height ($\Delta\nu_{1/2}$).

Table 9. Selected list of higher intensity vertical excitations computed at the TD-DFT/B3LYP//B3LYP/6-31G* level[a] for $[\mathbf{1a}]^{2+}$.

Excitation energy[a] (10^3 cm^{-1})[b]	Oscillator strength	ε[c]	$\psi_o \rightarrow \psi_v$[d]	Type of transition[e]
13.442 (743.91)	0.0648	4548.96	HOMO→LUMO+1 (0.67)[f]	dπ(Ru), π(BL_1^{2-})→dπ(Ru), π*(pap)
14.354 (696.64)	0.0229	1607.58	HOMO→LUMO (0.41)	dπ(Ru), π(BL_1^{2-})→dπ(Ru), π*(BL_1^{2-})
			HOMO→LUMO+4 (0.46)	dπ(Ru), π(BL_1^{2-})→dπ(Ru), π*(pap)
18.548 (539.14)	0.0990	6949.8	HOMO-2→LUMO (0.57)	dπ(Ru), π(BL_1^{2-})→dπ(Ru), π*(BL_1^{2-})
			HOMO-1→LUMO+2 (0.32)	dπ(Ru), π(BL_1^{2-})→dπ(Ru), π*(pap)
19.444 (514.30)	0.0455	3194.1	HOMO-5→LUMO+1 (0.17)	dπ(Ru)→dπ(Ru), π*(pap)
			HOMO-4→LUMO+2 (0.34)	dπ(Ru)→dπ(Ru), π*(pap)

[a] Singlet excitation energies. [b] Wavelength values in nm given in parentheses. [c] $M^{-1}cm^{-1}$. [d] Occupied and virtual orbitals. [e] BL_1^{2-} stands for the bridging ligand and pap represents the 2-(phenylazo)pyridine ligand. [f] Transition coefficients.

1500 nm (ε = 5000–11000 $M^{-1}cm^{-1}$) with a band width at half height ($\Delta\nu_{1/2}$) of 1900–3800 cm^{-1} (Figure 12 and Table 8). The experimentally obtained $\Delta\nu_{1/2}$ values are smaller than would be expected (3900–4300 cm^{-1}) from the Hush formula [$\Delta\nu_{1/2} = (2310\ E_{op})^{1/2}$][41] for a localized class-II mixed-valence system. This disagreement between experimental and calculated $\Delta\nu_{1/2}$ values and the high intensity of the NIR band supports the notion of a ligand-based oxidation to $Ru^{II}(\mu\text{-}BL^{\cdot-})Ru^{II}$ instead of metal-based oxidation to $Ru^{II}(\mu\text{-}BL^{2-})Ru^{III}$, as previously implied by the free-radi-

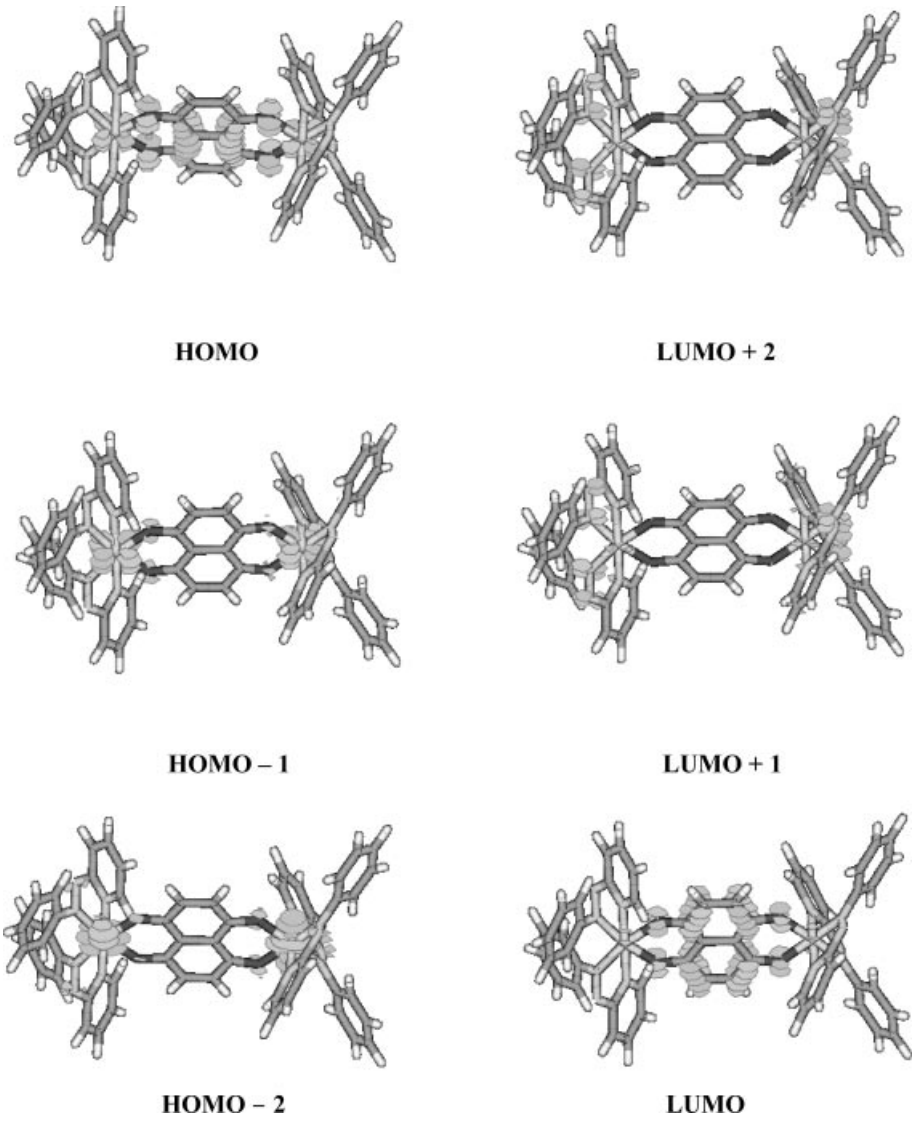

Figure 13. Kohn–Sham orbital contours of the frontier MOs of [**1a**]$^{2+}$ involved in the intense long-wavelength transitions.

cal EPR signal of [**1**–**8**]$^{3+}$ (Table 6). The low-energy NIR band is thus assigned as an intraligand transition involving the reduced component of the bridging ligand to the oxidized SOMO of its counterpart. Although the spectral features of [**8**]$^{2+/3+/4+}$ in the UV/Vis region are akin to those in other complexes, the expected NIR band for the intermediate [**8**]$^{3+}$ has not been detected (Figure 12, d, Table 8). On further oxidation to the spin-coupled diamagnetic Ru^{II}(μ-$BL^{\cdot-}$)Ru^{III} state in [**1**–**8**]$^{4+}$, the near-IR band disappears and the charge-transfer (MLCT/LMCT) bands are blue shifted. Unlike other complexes, the low-energy shoulder in [**7**]$^{4+}$ appears as an intense band at 892 nm (Table 8). The reduction of [**5**]$^{2+}$ to the radical species [**5**]$^{\cdot+}$ results in a red shift of the MLCT band from 561 to 597 nm with comparable intensity [Figure 12, c (inset), Table 8].

In summary, experimental results in combination with DFT calculations have established that the large quinonoid (BL^{2-})-bridged diruthenium complexes [$(aap)_2Ru^{II}$(μ-BL^{2-})$Ru^{II}(aap)_2$]$^{2+}$ [**1**–**8**]$^{2+}$ containing strongly π-accepting ancillary ligands (AL = arylazopyridine) undergo preferential first-step oxidation at the bridging ligand to give the paramagnetic radical-bridged diruthenium(II) species [$(aap)_2Ru^{II}$(μ-$BL^{\cdot-}$)$Ru^{II}(aap)_2$]$^{3+}$ [**1**–**8**]$^{3+}$. However, second-step oxidation selectively takes place at the metal center to give antiferromagnetically coupled singlet species, namely the mixed-valence $Ru^{II}Ru^{III}$ species [$(aap)_2Ru^{II}$(μ-$BL^{\cdot-}$)-$Ru^{III}(aap)_2$]$^{4+}$ [**1**–**8**]$^{4+}$, which are bridged by a radical bridging ligand (Scheme 4). Successive reductions, however, take place at the ligand centers. The first-step reduction process takes place either as a single electron transfer to the bridging ligand ($BL^{\cdot3-}$) or, in most cases, as a simultaneous two-electron transfer process involving the bridging ligand (μ-BL^{4-}) or a mixed situation of bridging ($BL^{\cdot3-}$) and ancillary ($aap^{\cdot-}$) ligands (Scheme 4).

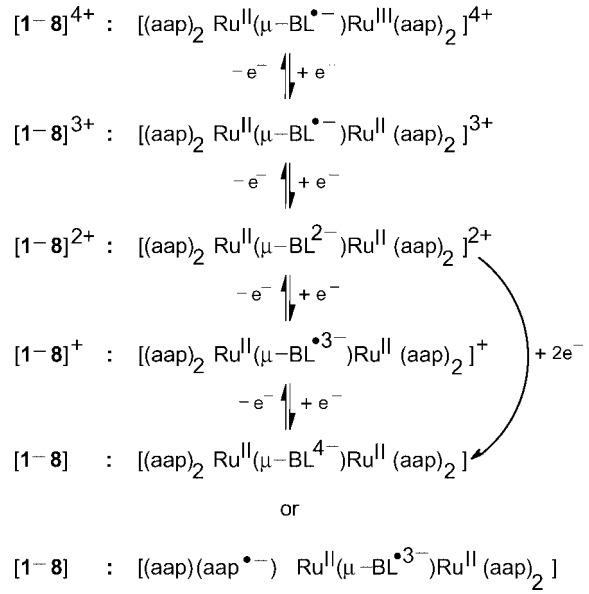

Scheme 4.

Experimental Section

Materials and Instrumentation: The precursor compounds *ctc*-$[Ru(aap)_2(H_2O)_2](ClO_4)_2{\cdot}H_2O$ and aap ligands were prepared according to the reported procedures.[42] The dinucleating ligand precursors 5,8-dihydroxy-1,4-napthoquinone (H_2BL_1), 2,3-dichloro-5,8-dihydroxy-1,4-napthoquinone (H_2BL_2), 6,11-dihydroxy-5,12-naphthacenedione (H_2BL_3), 1,4-dihydroxy-9,10-anthraquinone (H_2BL_4), 1,4-dihydroxy-2,3-dimethyl-9,10-anthraquinone (H_2BL_5), 6,7-dichloro-1,4-dihydroxy-9,10-anthraquinone (H_2BL_6), 1,4-diamino-9,10-anthraquinone (H_4BL_7), and 1,5-dihydroxy-9,10-anthraquinone (H_2BL_8) were purchased from Aldrich (USA). HPLC-grade solvents were used for spectroscopic and electrochemical studies. UV/Vis/NIR spectra in CH_3CN or CH_2Cl_2/0.1 M Et_4NClO_4 at 298 K were recorded with a Perkin–Elmer 950 lambda spectrophotometer. FT-IR spectra were recorded with a Nicolet spectrophotometer with samples prepared as KBr pellets. Solution electrical conductivity was checked using a Systronic 305 conductivity bridge. ^{1}H NMR spectra were obtained with a 300 or 400 MHz Varian FT spectrometer. The EPR measurements were made with a Varian model 109C E-line X-band spectrometer fitted with a quartz dewar for measurements at 77 K. Cyclic voltammetric, differential pulse voltammetric, and coulometric measurements were carried out using a PAR model 273A electrochemistry system. Platinum wire working and auxiliary electrodes and an aqueous saturated calomel reference electrode (SCE) were used in a three-electrode configuration. The supporting electrolyte was 0.1 M $[NEt_4]ClO_4$ and the solute concentration was about 10^{-3} M. The half-wave potential E°_{298} was set equal to $0.5(E_{pa} + E_{pc})$, where E_{pa} and E_{pc} are the anodic and cathodic cyclic voltammetric peak potentials, respectively. A platinum wire-gauze working electrode was used in the coulometric experiments. The elemental analyses were carried out with a Perkin–Elmer 240C elemental analyzer. Electrospray mass spectra were recorded with a Micromass Q-ToF mass spectrometer.

CAUTION! *Perchlorate salts of metal complexes with organic ligands are potentially explosive. Heating of dried samples must be avoided and handling of small amounts has to proceed with great caution using protection.*

Complexes [**1**–**8**]$(ClO_4)_2$ were prepared by following a general procedure. The details are given for [**1a**]$(ClO_4)_2$.

[(pap)$_2$Ru^{II}(μ-BL$_1^{2-}$)Ru^{II}(pap)$_2$](ClO$_4$)$_2$ [1](ClO$_4$)$_2$: The bridging ligand H_2BL_1 (0.013 g, 0.068 mmol) was added to the starting complex *ctc*-$[Ru(aap)_2(OH_2)_2](ClO_4)_2{\cdot}H_2O$ (0.1 g, 0.138 mmol) in absolute ethanol (20 mL) and the resulting mixture was heated to reflux under a dinitrogen atmosphere for 12 h. The initial purple solution gradually changed to violet. The solvent of the reaction mixture was then evaporated to dryness under reduced pressure. The resulting mixture was purified on a neutral alumina column. Initially, a blue compound corresponding to $[Ru(pap)_2Cl_2]$ was eluted with CH_2Cl_2/CH_3CN (15:1 v/v), followed by a violet compound with CH_2Cl_2/CH_3CN (5:1 v/v) corresponding to [**1a**]$(ClO_4)_2$. Evaporation of the solvent under reduced pressure yielded pure complex [**1a**]$(ClO_4)_2$. Yield: 0.046 g (50%). $C_{54}H_{40}Cl_2N_{12}O_{12}Ru_2$: calcd. C 49.02, H 3.05, N 12.71; found C 48.45, H 3.20, N 11.78. Λ_M (Ω^{-1} cm^2 M^{-1}) in acetonitrile at 25 °C: 219. IR (KBr disk): $\tilde{\nu}$ = 1089, 622 cm^{-1}. ^{1}H NMR (400 MHz, $CDCl_3$, 298 K): δ = 8.64 (d, J = 8.4 Hz, 1 H), 8.53 (d, J = 8.0 Hz, 1 H), 8.24 (t, J = 8.0, 7.9 Hz, 1 H), 8.13 (d, J = 5.2 Hz, 1 H), 8.08 (t, J = 7.2, 7.6 Hz, 1 H), 7.84 (d, J = 5.6 Hz, 1 H), 7.78 (t, J = 7.2, 7.6 Hz, 1 H), 7.6 (t, J = 7.2, 7.9 Hz, 1 H), 7.35 (m, 3 H), 7.18 (t, J = 7.6, 7.2 Hz, 3 H), 6.88 (d, J = 7.2 Hz, 2 H), 6.77 (t, J = 8.7, 6.4 Hz, 4 H) ppm.

[1b](ClO$_4$)$_2$: Yield: 0.041 g (45%). $C_{58}H_{48}Cl_2N_{12}O_{12}Ru_2$: calcd. C 50.50, H 3.51, N 12.19; found C 50.63, H 3.07, N 11.99. Λ_M (Ω^{-1} cm^2 M^{-1}) in acetonitrile at 25 °C: 214. IR (KBr disk): $\tilde{\nu}$ = 1088, 623 cm^{-1}. ^{1}H NMR (400 MHz, $CDCl_3$, 298 K): δ = 8.65 (d, J = 8.0 Hz, 1 H), 8.55 (d, J = 8.0 Hz, 1 H), 8.25 (q, J = 7.9, 7.6, 7.6 Hz, 1 H), 8.09 (t, J = 6.4, 7.6 Hz, 2 H), 7.82 (d, J = 5.2 Hz, 1 H), 7.76 (t, J = 6.0, 6.8 Hz, 1 H), 7.61 (t, J = 6.4, 6.0 Hz, 1 H), 7.15 (m, 2 H), 7.04 (m, 2 H), 6.87 (d, J = 5.2 Hz, 2 H), 6.57 (s, 2 H), 6.48 (m, 2 H), 2.17 (s, 3 H), 2.15 (s, 3 H) ppm.

[1c](ClO$_4$)$_2$: Yield: 0.039 g (42%). $C_{54}H_{36}Cl_6N_{12}O_{12}Ru_2$: calcd. C 44.45, H 2.49, N 11.53; found C 44.19, H 2.83, N 11.22. Λ_M (Ω^{-1} cm^2 M^{-1}) in acetonitrile at 25 °C: 236. IR (KBr disk): $\tilde{\nu}$ = 1090, 621 cm^{-1}. ^{1}H NMR (400 MHz, $CDCl_3$, 298 K): δ = 8.69 (d, J = 7.6 Hz, 1 H), 8.27 (t, J = 7.6, 6.8 Hz, 1 H), 7.92 (d, J = 5.2 Hz, 1 H), 7.69 (t, J = 6.0, 6.0 Hz, 1 H), 7.34 (m, 1 H), 7.16 (t, J = 8.0 Hz, 1 H), 6.89 (s, 1 H), 6.72 (d, J = 8.4 Hz, 1 H), 6.65 (s, 1 H) ppm.

[2](ClO$_4$)$_2$: Yield: 0.030 g (31%). $C_{54}H_{38}Cl_4N_{12}O_{12}Ru_2$: calcd. C 46.62, H 2.76, N 12.09; found C 46.45, H 2.89, N 11.83. Λ_M (Ω^{-1} cm^2 M^{-1}) in acetonitrile at 25 °C: 212. IR (KBr disk): $\tilde{\nu}$ = 1085, 623 cm^{-1}. ^{1}H NMR [400 MHz, $(CD_3)_2SO$, 298 K]: δ = 8.96 (t, J = 7.2, 5.6 Hz, 2 H), 8.34 (m, 2 H), 7.97 (m, 1 H), 7.75 (t, J = 6.0, 6.8 Hz, 1 H), 7.61 (m, 1 H), 7.44 (t, J = 4.8, 4.0 Hz, 2 H), 7.30 (t, J = 7.9, 6.0 Hz, 5 H), 6.94 (d, J = 15.9 Hz, 1 H), 6.85 (t, J = 9.5, 8.3 Hz, 2 H), 6.79 (t, J = 7.5, 7.9 Hz, 2 H) ppm.

[3](ClO$_4$)$_2$: Yield: 0.048 g (48%). $C_{62}H_{44}Cl_2N_{12}O_{12}Ru_2$: calcd. C 52.32, H 3.12, N 11.82; found C 52.36, H 3.22, N 11.50. Λ_M (Ω^{-1} cm^2 M^{-1}) in acetonitrile at 25 °C: 205. IR (KBr disk): $\tilde{\nu}$ = 1091, 623 cm^{-1}. ^{1}H NMR (400 MHz, $CDCl_3$, 298 K): δ = 8.68 (d, J = 8.0 Hz, 1 H), 8.59 (d, J = 7.6 Hz, 1 H), 8.25 (t, J = 6.8, 7.6 Hz, 1 H), 8.11 (t, J = 7.6 Hz, 1 H), 7.97 (m, 3 H), 7.75 (d, J = 4.8 Hz, 1 H), 7.69 (m, 4 H), 7.59 (t, J = 6.4, 6.0 Hz, 1 H), 7.49 (t, J = 5.6 Hz, 1 H), 7.41 (t, J = 7.6 Hz, 1 H), 7.24 (m, 2 H), 6.89 (t, J = 7.6, 5.2 Hz, 5 H) ppm.

[4](ClO$_4$)$_2$: Yield: 0.035 g (35%). $C_{58}H_{42}Cl_2N_{12}O_{12}Ru_2$: calcd. C 50.73, H 3.09, N 12.25; found C 50.64, H 3.29, N 12.01. Λ_M (Ω^{-1} cm^2 M^{-1}) in acetonitrile at 25 °C: 223. IR (KBr disk): $\tilde{\nu}$ = 1088, 622 cm^{-1}. ^{1}H NMR (400 MHz, $CDCl_3$, 298 K): δ = 8.68 (t, J = 8.6 Hz, 1 H), 8.61 (d, J = 8.1 Hz, 1 H), 8.55 (d, J = 7.8 Hz, 1 H),

8.26 (m, 2 H), 8.11 (m, 2 H), 7.93 (m, 2 H), 7.86 (d, J = 4.8 Hz, 1 H), 7.69 (m, 2 H), 7.38 (m, 3 H), 7.20 (m, 3 H), 6.96 (d, J = 6.3 Hz, 1 H), 6.86 (t, J = 6.0, 8.9 Hz, 1 H), 6.78 (t, J = 8.9, 6.0 Hz, 1 H) ppm.

[5](ClO$_4$)$_2$: Yield: 0.030 g (31%). $C_{60}H_{46}Cl_2N_{12}O_{12}Ru_2$: calcd. C 51.43, H 3.31, N 12.00; found C 50.94, H 3.38, N 11.92. Λ_M (Ω^{-1} cm^2 M^{-1}) in acetonitrile at 25 °C: 240. IR (KBr disk): $\tilde{\nu}$ = 1089, 623 cm^{-1}. ^{1}H NMR (400 MHz, $CDCl_3$, 298 K): δ = 8.67 (t, J = 8.1, 4.8 Hz, 1 H), 8.61 (d, J = 10.7 Hz, 1 H), 8.54 (d, J = 8.1 Hz, 1 H), 8.30 (t, J = 8.1, 7.8 Hz, 1 H), 8.19 (m, 1 H), 8.02 (t, J = 7.5, 8.1 Hz, 1 H), 7.93 (m, 1 H), 7.85 (d, J = 5.1 Hz, 1 H), 7.66 (m, 2 H), 7.39 (d, J = 7.5 Hz, 2 H), 7.19 (m, 4 H), 6.86 (t, J = 3.3, 5.1 Hz, 2 H), 6.76 (t, J = 6.0, 4.2 Hz, 2 H), 1.64 (s, 3 H) ppm.

[6](ClO$_4$)$_2$: Yield: 0.036 g (38%). $C_{58}H_{40}Cl_4N_{12}O_{12}Ru_2$: calcd. C 48.33, H 2.80, N 11.67; found C 48.65, H 2.93, N 11.43. Λ_M (Ω^{-1} cm^2 M^{-1}) in acetonitrile at 25 °C: 243. IR (KBr disk): $\tilde{\nu}$ = 1088, 622 cm^{-1}. ^{1}H NMR (400 MHz, $CDCl_3$, 298 K): δ = 8.66 (m, 1 H), 8.56 (t, J = 7.6, 6.4 Hz, 1 H), 8.25 (d, J = 11.1 Hz, 1 H), 8.19 (t, J = 8.4, 5.6 Hz, 1 H), 8.12 (t, J = 7.6, 7.9 Hz, 1 H), 8.02 (d, J = 5.6 Hz, 1 H), 7.92 (s, 1 H), 7.72 (m, 1 H), 7.61 (t, J = 5.6, 7.2 Hz, 1 H), 7.54 (m, 1 H), 7.20 (m, 3 H), 6.95 (d, J = 6.4 Hz, 1 H), 6.84 (t, J = 7.2, 7.9 Hz, 3 H), 6.78 (t, J = 6.4, 6.8 Hz, 3 H) ppm.

[7](ClO$_4$)$_2$: Yield: 0.030 g (34%). $C_{58}H_{44}Cl_2N_{14}O_{10}Ru_2$: calcd. C 50.80, H 3.24, N 14.31; found C 50.43, H 3.36, N 14.86. Λ_M (Ω^{-1} cm^2 M^{-1}) in acetonitrile at 25 °C: 239. IR (KBr disk): $\tilde{\nu}$ = 3260, 1087, 625 cm^{-1}. ^{1}H NMR (400 MHz, $CDCl_3$, 298 K): δ = 9.55 (s, NH), 8.65 (d, J = 6.0 Hz, 1 H), 8.53 (d, J = 6.0 Hz, 1 H), 8.08 (m, 3 H), 7.33 (d, J = 8.9 Hz, 2 H), 7.20 (m, 8 H), 6.98 (d, J = 7.5 Hz, 3 H), 6.84 (d, J = 7.2 Hz, 3 H) ppm.

[8](ClO$_4$)$_2$: Yield: 0.035 g (37%). $C_{58}H_{42}Cl_2N_{12}O_{12}Ru_2$: calcd. C 50.73, H 3.09, N 12.25; found C 50.62, H 3.38, N 12.33. Λ_M (Ω^{-1} cm^2 M^{-1}) in acetonitrile at 25 °C: 202. IR (KBr disk): $\tilde{\nu}$ = 1088, 622 cm^{-1}. ^{1}H NMR [400 MHz, $(CD_3)_2SO$, 298 K]: δ = 8.94 (m, 2 H), 8.32 (m, 2 H), 7.94 (m, 2 H), 7.46 (m, 4 H), 7.30 (m, 5 H), 7.21 (d, J = 8.0 Hz, 1 H), 7.06 (m, 1 H), 6.93 (d, J = 7.6 Hz, 2 H), 6.84 (d, J = 5.6 Hz, 2 H) ppm.

X-ray Crystallography: Single crystals of [**1a**](ClO$_4$)$_2$·H$_2$O and [**3**](ClO$_4$)$_2$ were grown by slow evaporation of a 1:1 dichloromethane/hexane solution. Data were collected with an OXFORD XCALIBUR-S CCD diffractometer (see Table 10 for further details). The structures were solved and refined by full-matrix least-squares techniques on F^2 with SHELX-97.[43] The absorption corrections were done by multi-scan (SHELXTL program package) and all the data were corrected for Lorentz polarization effects. Hydrogen atoms were included in the refinement process with a riding model. CCDC-606432 {[**1a**](ClO$_4$)$_2$·H$_2$O} and -606433 {[**3**](ClO$_4$)$_2$} contain the supplementary crystallographic data for this paper. These data can be obtained free of charge from The Cambridge Crystallographic Data Centre via www.ccdc.cam.ac.uk/data_request/cif.

Computational Details: Full geometry optimization of [**1a**]$^{2+}$ was carried out using the density functional theory method at the (R)B3LYP level.[44a,44b] All elements except ruthenium were assigned the 6-31G* basis set. The SDD basis set with effective core potential was employed for the ruthenium atoms.[44c,44d] Calculations were performed with Gaussian98 and Gaussian03.[44e,44f] Vertical electronic excitations based on B3LYP optimized geometries were computed using the time-dependent density functional theory (TD-DFT) formalism[44g] with the B3LYP functional using the above combination of basis sets. Molecular orbital compositions were analyzed using the AOMIX program.[44h–44j]

Table 10. Crystallographic data for [**1a**](ClO$_4$)$_2$·H$_2$O and [**3**](ClO$_4$)$_2$.

	[**1a**](ClO$_4$)$_2$·H$_2$O	[**3**](ClO$_4$)$_2$
Formula	$C_{27}H_{20}ClN_6O_7Ru$	$C_{31}H_{22}ClN_6O_6Ru$
M_r	677.01	711.07
Crystal size [mm]	0.33×0.26×0.21	0.15×0.10×0.10
Crystal system	monoclinic	orthorhombic
Space group	*C*2/*c*	*Pbca*
Z	8	8
a [Å]	35.069(5)	14.5179(18)
b [Å]	9.5143(13)	19.265(2)
c [Å]	19.5817(18)	22.516(3)
α [°]	90	90
β [°]	122.597(12)	90
γ [°]	90	90
V [Å^3]	5504.4(11)	6297.5(14)
$\rho_{calcd.}$ [g cm^{-3}]	1.634	1.500
T [K]	293(2)	293(2)
μ [mm^{-1}]	0.725	0.635
F(000)	2728	2872
hkl range	$-41 \le h \le 41$	$-17 \le h \le 17$
	$-11 \le k \le 11$	$-22 \le k \le 22$
	$-22 \le l \le 23$	$-26 \le l \le 26$
θ range [°]	2.98–25.00	3.00–25.00
Reflections collected	23331	24895
Unique reflections [R_{int}]	4779 [0.0224]	5533 [0.0572]
Data/restraints/parameters	4779/14/388	5533/0/406
*R*1 [$I > 2\sigma(I)$]	0.0475	0.0621
*wR*2 [all data]	0.1424	0.1909
Goodness-of-fit	1.076	0.910
Residual electron density [e Å^{-3}]	0.872, –0.714	1.328, –0.429

Supporting Information (for details see the footnote on the first page of this article): Kohn−Sham orbitals of [**1a**]$^{2+}$ (Figure S1); optimized coordinates for BL_1^{2-} (Table S1), pap (Table S2) and [**1a**]$^{2+}$ (Table S3); calculated bond lengths and angles of [**1a**]$^{2+}$ (Table S4) and TD-DFT data for [**1a**]$^{2+}$ (Table S5).

Acknowledgments

Financial support received from the Department of Science and Technology, and Council of Scientific and Industrial Research, New Delhi (India) is gratefully acknowledged. X-ray structural studies for [**1a**](ClO$_4$)$_2$ and [**3**](ClO$_4$)$_2$ were carried out at the National Single Crystal Diffractometer Facility, Indian Institute of Technology, Bombay. Special acknowledgment is made to the Sophisticated Analytical Instrument Facility (SAIF) and the Computer Center, Indian Institute of Technology Bombay, respectively, for providing the EPR and computational facilities.

[1] a) W. Kaim, A. Klein, M. Glöckle, *Acc. Chem. Res.* **2000**, *33*, 755; b) M. D. Ward, *Chem. Soc. Rev.* **1995**, *24*, 121; c) J. A. McCleverty, M. D. Ward, *Acc. Chem. Res.* **1998**, *31*, 842; d) R. J. Crutchley, in *Comprehensive Coordination Chemistry II* (Eds.: J. A. McCleverty, T. J. Meyer), **2004**, vol. 2, pp. 235; e) J. T. Hupp, in *Comprehensive Coordination Chemistry II* (Eds.: J. A. McCleverty, T. J. Meyer), **2004**, vol. 2, pp. 709; f) B. K. Breedlove, T. Yamaguchi, T. Ito, C. H. Londergan, C. P. Kubiak, in *Comprehensive Coordination Chemistry* II (Eds.: J. A. McCleverty, T. J. Meyer), **2004**, vol. 2, pp. 717; g) G. Giuffrida, S. Campagna, *Coord. Chem. Rev.* **1994**, *135–136*, 517; h) B. S. Brunschwig, C. Creutz, N. Sutin, *Chem. Soc. Rev.* **2002**, *31*, 168.

[2] a) V. Balzani, M. Venturi, A. Credi, in *Molecular Devices and Machines*: *A Journey into the Nanoworld*, Wiley-VCH, Weinheim, Germany, **2003**; b) B. L. Feringa, in *Molecular Switches*, Wiley-VCH, Weinheim, Germany, **2001**; c) F. Paul, C. Lapinte, *Coord. Chem. Rev.* **1998**, *178–180*, 431; d) M. D. Ward, *Chem. Ind.* **1997**, 640; e) M. D. Ward, *Chem. Ind.* **1996**, 568; f) O. Kahn, J.-P. Launay, *Chemtronics* **1988**, *3*, 140; g) S. Fraysse, C. Coudret, J.-P. Launay, *J. Am. Chem. Soc.* **2003**, *125*, 5880; h) S. Fraysse, C. Coudret, J.-P. Launay, *Eur. J. Inorg. Chem.* **2000**, *7*, 1581; i) M. D. Ward, *J. Chem. Educ.* **2001**, *78*, 321.

[3] a) B. S. Brunschwig, N. Sutin, *Coord. Chem. Rev.* **1999**, *187*, 233; b) A. Bencini, I. Ciofini, C. A. Daul, A. Ferretti, *J. Am. Chem. Soc.* **1999**, *121*, 11418.

[4] a) D. E. Richardson, H. Taube, *Coord. Chem. Rev.* **1984**, *60*, 107; b) C. E. B. Evans, M. L. Naklicki, A. R. Rezvani, C. A. White, V. V. V. Kondratiev, R. J. Crutchley, *J. Am. Chem. Soc.* **1998**, *120*, 13096; c) F. Barriere, N. Camire, W. E. Geiger, U. T. Mueller-Westerhoff, R. Sanders, *J. Am. Chem. Soc.* **2002**, *124*, 7262; d) G. M. Brown, N. Sutin, *J. Am. Chem. Soc.* **1979**, *101*, 883.

[5] a) M. Al-Noaimi, G. P. A. Yap, R. J. Crutchley, *Inorg. Chem.* **2004**, *43*, 1770; b) K. D. Demadis, C. M. Hartshorn, T. J. Meyer, *Chem. Rev.* **2001**, *101*, 2655.

[6] S. Ghumaan, B. Sarkar, S. Patra, J. van Slageren, J. Fiedler, W. Kaim, G. K. Lahiri, *Inorg. Chem.* **2005**, *44*, 3210.

[7] A. Shukla, A. Das, *Polyhedron* **2000**, *19*, 2605.

[8] S. Kar, B. Sarkar, S. Ghumaan, D. Janardanan, J. van Slageren, J. Fiedler, V. G. Puranik, R. B. Sunoj, W. Kaim, G. K. Lahiri, *Chem. Eur. J.* **2005**, *11*, 4901.

[9] M. D. Ward, *Inorg. Chem.* **1996**, *35*, 1712.

[10] a) A. Dei, D. Gatteschi, L. Pardi, *Inorg. Chem.* **1990**, *29*, 1442; b) S. Bruni, F. Cariati, A. Dei, D. Gatteschi, *Inorg. Chim. Acta* **1991**, *186*, 157.

[11] G. G. Sadler, N. R. Gordon, *Inorg. Chim. Acta* **1991**, *180*, 271.

[12] H. Masui, A. L. Freda, M. C. Zerner, A. B. P. Lever, *Inorg. Chem.* **2000**, *39*, 141.

[13] L. F. Joulie, E. Schatz, M. D. Ward, F. Weber, L. J. Yellowlees, *J. Chem. Soc., Dalton Trans.* **1994**, 799.

[14] S. Patra, B. Sarkar, S. Ghumaan, J. Fiedler, S. Zalis, W. Kaim, G. K. Lahiri, *Dalton Trans.* **2004**, *5*, 750.

[15] P. R. Auburn, A. B. P. Lever, *Inorg. Chem.* **1990**, *29*, 2551.

[16] S. Joss, H. Reust, A. Ludi, *J. Am. Chem. Soc.* **1981**, *103*, 981.

[17] a) S. Patra, B. Sarkar, S. M. Mobin, W. Kaim, G. K. Lahiri, *Inorg. Chem.* **2003**, *42*, 6469; b) P. Ghosh, A. Begum, D. Herebian, E. Bothe, K. Hildenbrand, T. Weyhermüller, K. Wieghardt, *Angew. Chem.* **2003**, *115*, 581; *Angew. Chem. Int. Ed.* **2003**, *42*, 563; c) K. S. Min, T. Weyhermüller, K. Wieghardt, *Dalton Trans.* **2003**, 1126; d) C. Remenyi, M. Kaupp, *J. Am. Chem. Soc.* **2005**, *127*, 11399; e) H. Chun, E. Bill, E. Bothe, T. Weyhermüller, K. Wieghardt, *Inorg. Chem.* **2002**, *41*, 5091; f) W. Kaim, M. Wanner, A. Knödler, S. Zalis, *Inorg. Chim. Acta* **2002**, *337*, 163; g) C. G. Pierpont, *Coord. Chem. Rev.* **2001**, *219–221*, 415; h) P. Chaudhuri, C. N. Verani, E. Bill, E. Bothe, T. Weyhermüller, K. Wieghardt, *J. Am. Chem. Soc.* **2001**, *123*, 2213; i) C. G. Pierpont, A. S. Attia, *Collect. Czech. Chem. Commun.* **2001**, *66*, 33; j) J. Rall, M. Wanner, M. Albrecht, F. M. Hornung, W. Kaim, *Chem. Eur. J.* **1999**, *5*, 2802; k) C. N. Verani, S. Gallert, E. Bill, T. Weyhermüller, K. Wieghardt, P. Chaudhuri, *Chem. Commun.* **1999**, 1747; l) M. Ebadi, A. B. P. Lever, *Inorg. Chem.* **1999**, *38*, 467; m) J. Rall, E. Waldhör, B. Schwederski, M. Schwach, S. Kohlmann, W. Kaim, in *Bioinorganic Chemistry: Transition Metals in Biology and their Coodination Chemistry* (Ed.: A. X. Trautwein), VCH, Weinheim, **1997**, pp. 476; n) R. A. Metcalfe, A. B. P. Lever, *Inorg. Chem.* **1997**, *36*, 4762; o) G. Speier, A. Whalen, J. Csihony, C. G. Pierpont, *Inorg. Chem.* **1995**, *34*, 1355; p) C. G. Pierpont, C. W. Lange, *Prog. Inorg. Chem.* **1994**, *41*, 331; q) J. Rall, W. Kaim, *J. Chem. Soc., Faraday Trans.* **1994**, *90*, 2905; r) H. Masui, A. B. P. Lever, E. S. Dodsworth, *Inorg. Chem.* **1993**, *32*, 258; s) B. Schwederski, W. Kaim, *Inorg. Chim. Acta* **1992**, *195*, 123; t) N. Bag, G. K. Lahiri, P. Basu, A. Chakravorty, *J. Chem. Soc., Dalton Trans.* **1992**, 113; u) H. Masui, A. B. P. Lever, P. Auburn, *Inorg. Chem.* **1991**, *30*, 2402; v) S. Ernst, P. Hänel, J. Jordanov, W. Kaim, V. Kasack, E. Roth, *J. Am. Chem. Soc.* **1989**, *111*, 1733; w) S. Ernst, V. Kasack, C. Bessenbacher, W. Kaim, *Z. Naturforsch., Teil B* **1987**, *42*, 425; x) M. Haga, E. S. Dodsworth, A. B. P. Lever, *Inorg. Chem.* **1986**, *25*, 447; y) R. B. Salmonsen, A. Abelleira, M. J. Clarke, *Inorg. Chem.* **1984**, *23*, 387; z) A. Dei, D. Gatteschi, C. Sangregorio, L. Sorace, *Acc. Chem. Res.* **2004**, *37*, 827.

[18] a) B. Sarkar, S. Patra, J. Fiedler, R. B. Sunoj, D. Janardanan, S. M. Mobin, M. Niemeyer, G. K. Lahiri, W. Kaim, *Angew. Chem. Int. Ed.* **2005**, *44*, 5655; b) J. A. Zampese, F. R. Keene, P. J. Steel, *Dalton Trans.* **2004**, 4124.

[19] S. Patra, B. Mondal, B. Sarkar, M. Niemeyer, G. K. Lahiri, *Inorg. Chem.* **2003**, *42*, 1322.

[20] G. K. J. Chao, R. L. Sime, R. J. Sime, *Acta Crystallogr., Sect. B* **1973**, *29*, 2845.

[21] S. Kar, N. Chanda, S. M. Mobin, F. A. Urbanos, M. Niemeyer, V. G. Puranik, R. Jimenez-Aparicio, G. K. Lahiri, *Inorg. Chem.* **2005**, *44*, 1571.

[22] A. Seal, S. Ray, *Acta Crystallogr., Sect. C* **1984**, *40*, 929.

[23] B. K. Santra, G. A. Thakur, P. Ghosh, A. Pramanik, G. K. Lahiri, *Inorg. Chem.* **1996**, *28*, 3050.

[24] a) A. Mostad, C. Romming, *Acta Chem. Scand.* **1971**, *25*, 3561; b) C. H. Chang, R. F. Porter, S. H. Bauer, *J. Am. Chem. Soc.* **1970**, *92*, 5313; c) S. P. Sengupta, T. Roy, *Cryst. Struct. Commun.* **1980**, *9*, 965; d) N. Bag, A. Pramanik, G. K. Lahiri, A. Chakravorty, *Inorg. Chem.* **1992**, *31*, 40; e) R. A. Krause, K. Krause, *Inorg. Chem.* **1982**, *21*, 1714; f) A. K. Deb, P. C. Paul, S. Goswami, *J. Chem. Soc., Dalton Trans.* **1988**, 2051; g) A. Saha, C. Das, S. Goswami, S.-M. Peng, *Indian J. Chem. Sect. A* **2001**, *40*, 198.

[25] K. Heinze, S. Mann, G. Huttner, L. Zsolnai, *Chem. Ber.* **1996**, *129*, 115.

[26] S. Arnold, V. Mansel, G. Klar, *Z. Naturforsch., Teil B* **1990**, *45*, 369.

[27] C. G. Pierpont, L. C. Francesconi, D. N. Hendrickson, *Inorg. Chem.* **1978**, *17*, 3470.

[28] M. J. Maroney, R. O. Day, T. Psyris, L. M. Fleury, J. P. Whitehead, *Inorg. Chem.* **1989**, *28*, 173.

[29] A. Elduque, F. Aguilera, F. J. Lahoz, J. A. Lopez, L. A. Oro, M. T. Pinillos, *Inorg. Chim. Acta* **1998**, *274*, 15.

[30] a) A. Bharath, B. K. Santra, P. Munshi, G. K. Lahiri, *J. Chem. Soc., Dalton Trans.* **1998**, 2643; b) B. K. Santra, G. K. Lahiri, *J. Chem. Soc., Dalton Trans.* **1998**, 139; c) B. K. Santra, G. K. Lahiri, *J. Chem. Soc., Dalton Trans.* **1997**, 129.

[31] C. Creutz, *Prog. Inorg. Chem.* **1983**, *30*, 1.

[32] S. Patra, T. A. Miller, B. Sarkar, M. Niemeyer, M. D. Ward, G. K. Lahiri, *Inorg. Chem.* **2003**, *42*, 4707.

[33] B. Mondal, M. G. Walawalkar, G. K. Lahiri, *J. Chem. Soc., Dalton Trans.* **2000**, 4209.

[34] N. Chanda, B. Sarkar, J. Fiedler, W. Kaim, G. K. Lahiri, *Dalton Trans.* **2003**, 3550.

[35] S. Patra, B. Sarkar, S. Maji, J. Fiedler, F. A. Urbanos, R. Jimenez-Aparicio, W. Kaim, G. K. Lahiri, *Chem. Eur. J.* **2006**, *12*, 489.

[36] S. Chakraborty, R. H. Laye, R. L. Paul, R. G. Gonnade, V. G. Puranik, M. D. Ward, G. K. Lahiri, *J. Chem. Soc., Dalton Trans.* **2002**, 1172.

[37] B. Mondal, H. Paul, V. G. Puranik, G. K. Lahiri, *J. Chem. Soc., Dalton Trans.* **2001**, 481.

[38] a) S. Patra, B. Sarkar, S. Ghumaan, J. Fiedler, W. Kaim, G. K. Lahiri, *Dalton Trans.* **2004**, 754; b) N. Chanda, R. H. Laye, S. Chakraborty, R. L. Paul, J. C. Jeffery, M. D. Ward, G. K. Lahiri, *J. Chem. Soc., Dalton Trans.* **2002**, 3496; c) S. Patra, B. Sarkar, S. Ghumaan, J. Fiedler, W. Kaim, G. K. Lahiri, *Inorg. Chem.* **2004**, *43*, 6108.

[39] a) J. M. Villegas, S. R. Stoyanov, W. Huang, L. J. Lockyear, J. H. Reibenspies, D. P. Rillema, *Inorg. Chem.* **2004**, *43*, 6383; b) S. R. Stoyanov, J. M. Villegas, D. P. Rillema, *Inorg. Chem.* **2002**, *41*, 2941; c) S. R. Stoyanov, J. M. Villegas, D. P. Rillema, *Inorg. Chem. Commun.* **2004**, *7*, 838.
[40] Conversion of calculated oscillator strength to molar absorptivity was done based on the following references: a) R. S. Drago, in *Physical Methods for Chemists*, 2nd ed., Saunders College Publishing, Ft. Worth, Texas, **1992**; b) J. E. Monat, J. H. Rodriguez, J. K. McCusker, *J. Phys. Chem. A* **2002**, *106*, 7399.
[41] N. S. Hush, *Prog. Inorg. Chem.* **1967**, *8*, 391.
[42] S. Goswami, A. R. Chakravarty, A. Chakravorty, *Inorg. Chem.* **1983**, *22*, 602.
[43] G. M. Sheldrick, *SHELXS-97*, Program for Crystal Structure Solution and Refinement, University of Göttingen, Germany, **1997**.
[44] a) A. D. Becke, *Phys. Rev. A* **1988**, *38*, 3098; b) C. Lee, W. Yang, R. G. Parr, *Phys. Rev. B* **1988**, *37*, 785; c) D. Andrae, U. Haeussermann, M. Dolg, H. Stoll, H. Preuss, *Theor. Chim. Acta* **1990**, *77*, 123; d) P. Fuentealba, H. Preuss, H. Stoll, L. V. Szentpaly, *Chem. Phys. Lett.* **1989**, *89*, 418; e) M. J. Frisch, et al. *Gaussian03*, revision C.02; Gaussian, Inc.: Wallingford CT, **2004**; f) Frisch et al. *Gaussian 98*, revision A.11. 4; Gaussian, Inc.: Pittsburgh, PA, **1998**; g) M. Casida, in *Recent Advances in Density Functional Methods* (Ed.: D. P. Chong), World Scientific Press, Singapore, **1995**, vol. I, pp. 155; h) G. Schaftenaar, J. H. Noordik, *J. Comput.-Aided Mol. Design* **2000**, *14*, 123; i) S. I. Gorelsky, *AOMIX* program, http://www.sg-chem.net/; j) S. I. Gorelsky, A. B. P. Lever, *J. Organomet. Chem.* **2001**, *635*, 187.

Received: May 3, 2006
Published Online: August 24, 2006

